



## OPEN Micro hole drilling and multi criteria optimization of soda lime glass via ultrasonic assisted rotary electrochemical discharge drilling

Sahil Grover<sup>1</sup>, Viveksheel Rajput<sup>1</sup>, Sanjay Kumar Mangal<sup>1</sup>, Sarbjit Singh<sup>1</sup>, Sandeep Singh<sup>2,3</sup>, Shubham Sharma<sup>4,5,6</sup>, Ehab El Sayed Massoud<sup>7</sup>, Dražan Kozak<sup>8</sup> & Jasmina Lozanovic<sup>9</sup>

Regardless of the materials' intrinsic characteristics, electrochemical discharge drilling (ECDD) effectively micro-machines various materials. The present article optimizes the ultrasonic assisted rotary ECDD (UR-ECDD) process for maximizing the material removal rate (MRR), while minimizing the hole overcut (HOC) and circularity error (CE). The micro-holes are produced using a Taguchi's L16 array and multi-criteria optimization is carried out using grey relational based analysis (GRA). MRR, HOC and CE serve as a response parameter while tool vibration, tool feed rate, working material rotation, applied voltage and electrolyte concentration are control variables. UR-ECDD results in the improvement of 14.8% in MRR, 15.4% in HOC and 17.2% in CE when compared to the ECDD process. The optimized control variables based on GRA are derived as A4C3B4D1E4 (6  $\mu\text{m}$ , 80 rpm, 0.9 mm/min, 35 V, 25 wt%). Tool vibration emerged as the most significant control variable. The GRG's predicted results at optimum conditions provide a satisfactory alignment with the experimental results. Machine learning-based algorithms are also used to predict the responses using Random Forest and Gradient Boost approaches. Comparative results indicated that the Random Forest predicts the responses with reduced error in comparison to the Gradient Boost method. The validation of the dataset exhibits a similar trend confirming the efficacy of prediction.

**Keywords** Ultrasonic assisted rotary, Machine learning, Optimization, Overcut, Sparks, Multi-criteria, Circularity

The hybrid Electrochemical Discharge Drilling (ECDD) utilizes the thermal heat generated by sparks to remove work material in the initial stages of micro-hole drilling, followed by chemical dissolution. This method was initially outlined by Kurafuji and Suda<sup>1</sup> in 1968, primarily in the context of drilling glass. They underscored the possibility for efficiently drilling tiny holes with a high rate of material removal in glass materials. Since then, a significant amount of empirical and analytical research on the ECDD process has been published to improve its use in different applications with respect to glass materials. Glass is a widely used functional material in the electrical industry for a variety of purposes. It is essential to the manufacture of microdevices such as solid oxide fuel cells for portable electronic devices, pumps, and reactors as well as the packaging of micro-electromechanical systems (MEMS) devices and microelectronic packaging<sup>2</sup>. In semiconductor applications, glass is an essential substrate for bonding with wafers, enabling the integration of different electrical components<sup>3</sup>. ECDD process exhibits various applications such as glass micro-holes and 3D micro-feature fabrication: an essential

<sup>1</sup>Mechanical Engineering Department, Punjab Engineering College, Chandigarh 160012, India. <sup>2</sup>School of Engineering, Bhara University, Waknaghat, Solan, Himachal Pradesh 173234, India. <sup>3</sup>Faculty of Engineering, Sohar University, PO Box 44, PCI 311 Sohar, Oman. <sup>4</sup>Department of Technical Sciences, Western Caspian University, Baku, Azerbaijan. <sup>5</sup>Centre for Research Impact and Outcome, Chitkara University Institute of Engineering and Technology, Chitkara University, Rajpura, Punjab 140401, India. <sup>6</sup>Jadara University Research Center, Jadara University, Irbid, Jordan. <sup>7</sup>College of Applied Sciences, King Khalid University, Dhahran Al-Janoub, Kingdom of Saudi Arabia. <sup>8</sup>Mechanical Engineering Faculty in Slavonski Brod, University of Slavonski Brod, Trg Ivane Brlić-Mažuranić 2, 35000 Slavonski Brod, Croatia. <sup>9</sup>Department of Engineering, University of Applied Sciences - FH Campus Wien, 1100 Vienna, Austria. ✉email: drsandeep1786@gmail.com; shubham543sharma@gmail.com; shubhamsharmacsirciri@gmail.com; jasmina.lozanovic@fh-campuswien.ac.at

technique for MEMS and related industries including astronomy, kitchenware, and microbiological labs<sup>4</sup>. Glass micro texturing for use in micro-fluidic device applications, including mini-bioreactors, digital micromirrors, and single-cell capture devices<sup>5</sup>.

### Literature review

Basak and Ghosh<sup>6</sup> successfully illustrated the spark mechanism in the ECDD process. They emphasized that the sparking phenomenon closely resembles the action of the switch. Sundaram et al.<sup>7</sup> investigated the formation of a gas film around the tool electrode and its impact on machining quality, specifically assessing hole diameter and overcut. ECDD process, comprising three key elements: the primary tool, secondary and the working material submerged in an electrolyte solution. The setup arrangement involves a defined gap distance across the two tools while maintaining a slight vertical offset (machining gap) distance of the primary tool from the working material. The primary tool, with smaller dimensions than the secondary tool, ensures enhanced spark uniformity. With the creation of a potential difference using voltage application, electrolysis and other electrochemical processes have been started. Tiny oxygen-hydrogen bubbles occur at the secondary and primary tools, grow into bigger bubbles, and surround the primary tool to create a gas layer. The disintegration of the gas layer causes the spark to start. The work material can be removed more easily by chemical etching and heat infusion from sparks when the voltage is increased since it increases bubble formation and current densities<sup>8,9</sup>. Bhattacharyya et al.<sup>10</sup> investigated working material removal techniques and found prospects for improved machining performance. In various investigations using adaptive tool feed in ECDD, Rajput et al.<sup>11–13</sup> investigated the production of micro-holes in a quartz and glass material with improved geometrical features using ECDD process.

The application of the ultrasonic vibration ensures a continuous flow of electrolyte and consistent uniform spark distribution in the electrochemical discharge-based drilling process. Hung et al.<sup>14</sup> recently investigated the use of hybrid technology combining ultrasonic-assisted electrochemical discharge grinding with in-situ ultrasonic broaching. An array of square microholes were successfully created with enhanced geometric features on quartz glass using this cutting-edge method. Rusli and Furutani<sup>15</sup> discovered that incorporating ultrasonic vibrations to the tool electrode improved discharge behaviour and electrolyte circulation, resulting in greater surface quality of soda lime glass. Their findings indicated that applying ultrasonic assistance to the tool electrode improves machining efficiency by forming a thin gas layer and increasing the number of discharges under constant circumstances<sup>16,17</sup>. Wuthrich et al.<sup>18</sup> vibrated the tool with a current-controlled voice-coil actuator with a range of 0–30  $\mu\text{m}$  and a frequency range of 0–30 Hz. The investigation discovered that holes on a glass materials occurred in less than 10 s in the hydrodynamic regime. Effective electrolyte flushing, principally generated by vibrations was the significant contributor to this efficiency. The assistance of the rotation to the ECDD process can further enhances the MRR, quality of machined surface and dimensional improvement. By preventing discharge focus at a single spot with high-speed rotation, only the area below the tool electrode may be machined. This reduces stray corrosion and gives the hole's entrance accurate dimensions. Large amounts of hydrogen bubbles and sludge can be removed from the space under the tool electrode by speeding up the rotation. This improvement aids in better electrochemical processes, which eventually increase the quality of the machining. It has been demonstrated that the application of ultrasonic vibrations can raise the hole depth in alumina by as much as 52%<sup>19</sup> and, greatly enhance the machining quality of microstructures on glass work material<sup>20</sup> in comparison to traditional ECDD.

Fan et al.<sup>21</sup> investigated at how the rotation affected the overcut and conicity of holes in ECDD process. According to the research, rotating the tool produced holes with good circularity, but using stationary tools produced holes with low circularity. Apart from rotational effect, various experimental studies have been reported to find the effect of different control variables such as voltage, concentration and tool feed rate during glass machining<sup>22</sup>. The results of the experiments showed that the applied voltage had a substantial effect on both material removal and tool wear. The results showed that higher applied voltages are related to more prominent thermal fractures. The concentration of the electrolyte, which affected its viscosity, is important since higher concentrations resulted in smoother machined surfaces because they had stronger chemical etching effects<sup>23</sup>. Singh et al.<sup>24</sup> successfully machined micro-holes in a silicon wafer material using ECDD process and concluded that tool feed rate plays a significant role in determining the hole characteristics. The tool electrode feed mechanism is also reported as a crucial factor in how much material is removed during the ECDD process. The tool electrode is continually transported towards the workpiece at a constant pace in the constant velocity feed mechanism, preventing any direct physical contact between the tool electrode and the workpiece. In order to maximise the rate of material removal, Gautam and Jain<sup>25</sup> employed constant velocity feed rates together with the application of the rotational effect. They also highlighted the competitive advantages of constant velocity tool electrode feed mechanisms as opposed to gravity feed mechanisms. Many experimental findings in ECDD process showcase the application of the optimization techniques to identify the set of optimum values of the control variables<sup>26–28</sup>. Wang et al.<sup>29</sup> recently carried out a multi-response optimization investigation to find the optimum parameters for reducing the overcut, and surface roughness of glass material with respect to different control variables during ECDG process. Bindu et al.<sup>30</sup> utilized the Grey Relational Analysis (GRA) to identify the optimum control variables in ECDD process for maximizing the removal rate of quartz material and minimizing the TWR. ECDD performance. Bellubbi et al.<sup>31</sup> successfully applied GRA facilitated multi-criteria optimization, identifying the optimal parameters as 25 wt%, 45 V, 45  $\mu\text{s}$  pulse on time, 400 Hz pulse frequency and 1.5 mm standoff distance during micro-channeling of the silica glass using the ECDD process.

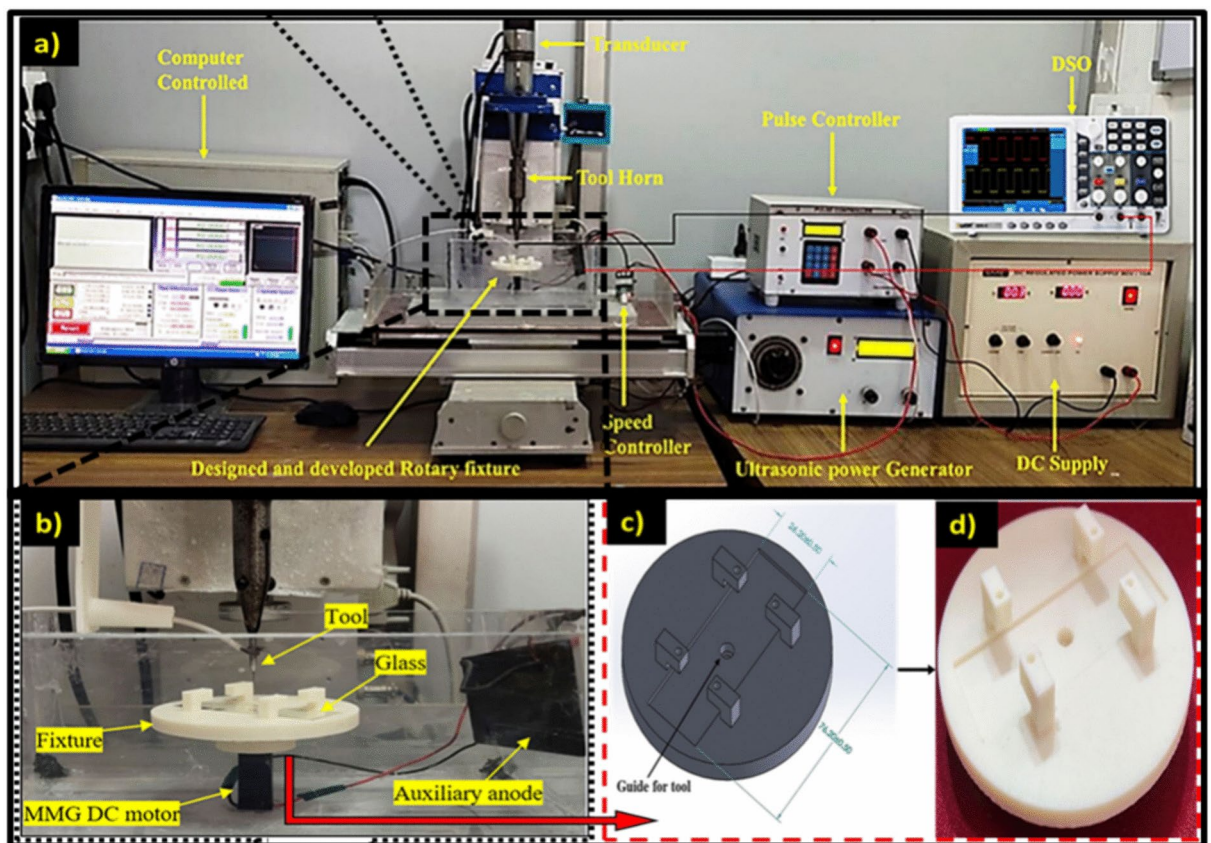
### Problem formulation

According to the literature, a large number of thorough research have been performed to assess the ECDD process with HOC and CE as the response parameters. But still some challenges exist during the soda lime glass drilling with the ECDD process i.e., low MRR at higher depths, poor circularity due to non-uniform sparks and

tool wear during the machining process, high HOC because of discontinuous material removal pattern resulting from unstable gas film formation. ECDD generally results in unstable and inconsistent spark generation due to a lack of electrolyte availability since the electrolyte evaporates during the process. Thus, the need is there to address these challenges that enhance the electrolyte replenishment and result in constant spark around the tool. As a result, enhanced responses will be obtained. While extensive literature exists on the effect of control variables on response variables in the ECDD process, few studies have reported on the performance analysis of the UR-ECDD process concerning multi-response indicators like MRR, HOC, and CE. Moreover, the multi-response optimization of the UR-ECDD process using GRA for maximizing MRR and minimizing HOC & CE with the work material rotation has never reported to date. This paper investigates the novel investigation of evaluating the impact of control variables like tool vibrations, work material rotational speed, tool feed rate, electrolyte concentration and applied voltage during micro-hole fabrication on a glass material using (UR-ECDD). Furthermore, it utilizes GRA for multi-criteria optimization to determine the optimal combinations of control variables.

### Experimental setup and process capability

A novel method of micro-hole drilling is introduced by the designing and developing the ultrasonic assisted and rotary work material electrochemical discharge-based drilling process (UR-ECDD) equipment as shown in Fig. 1. The setup is equipped with HY3040 CNC machine and computer-controlled software. It consists of an ultrasonic power generator that provides a piezoelectric transducer with frequencies higher than 20 kHz. The electrical impulses are converted by this transducer into ultrasonic vibrations with a small amplitude, which are subsequently sent through the tool horn to the tool end. It further takes into account the working material rotational speed application during the micro-hole drilling operation. The MMG DC motor ranging from 0 to 100 RPM is used for rotating the fixture on which the glass material is attached. The rotation of the work material causes the seepage action which provides the additional stability to the hydrogen gas film formation as well as spark generated during the process. The tool and auxiliary anode receive voltage from the DC power source. The X and Y axis motions and the tool feed rate are controlled by the CNC programme. Figure 1 gives viewers a visual understanding of the arrangement and parts used in this sophisticated machining procedure. Figure 1b, c displays the real picture of the fixture that is developed using Solidworks and fabricated using a 3D printer. The bottom and side walls, along with the other five sides, provide sufficient support for the work material in the fixture design.



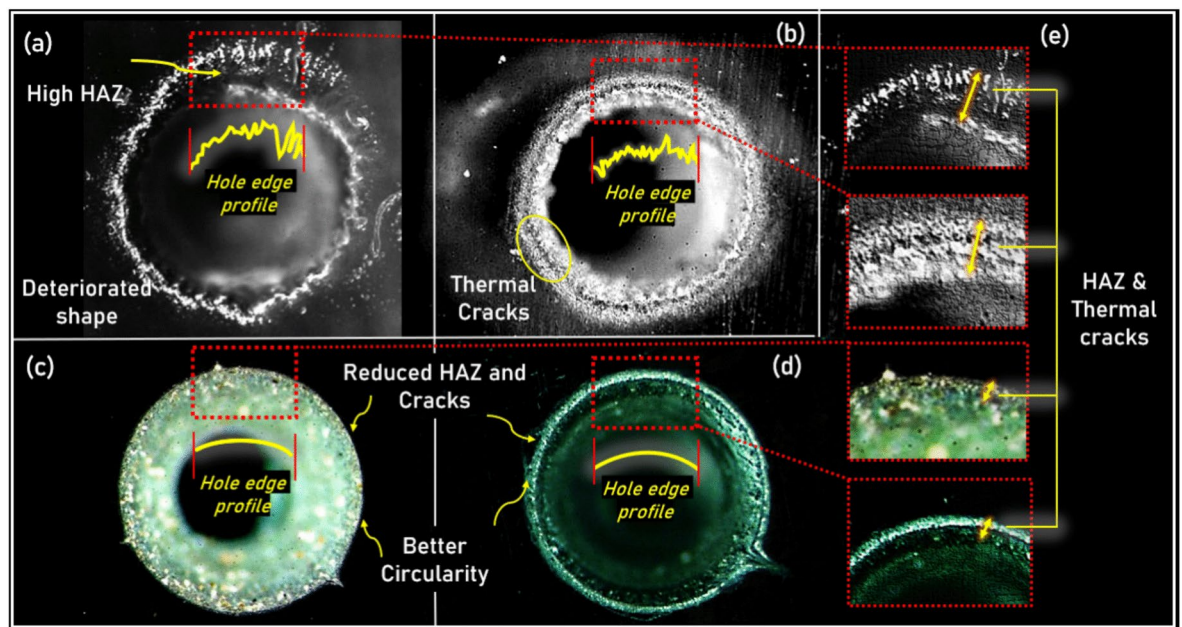
**Fig. 1.** (a) Developed experimental setup of UR-ECDD process (b) fabricated rotational work material holding fixture (c) CAD model of the rotational work material holding fixture (d) zoomed view.

Figure 2 shows the comparative microscopy images of the micro-holes drilled with conventional ECDD process and UR-ECDD process. A much-deteriorated hole shape with large number of thermal cracks and Heat affected zone (HAZ) is produced using ECDD process (Fig. 2a, b). It is noticed that the combined application of tool electrode vibrations and work material rotation produces a better micro-hole geometry in terms of overcut, HAZ, thermal cracks and circularity (Fig. 2c–e). An improvement of 14.8% in MRR, 15.4% in HOC and 17.2% in CE is observed with the application of UR-ECDD process when compared to ECDD process at 40 V, 10 wt% NaOH concentration, 0.8 mm/min feed rate, 6  $\mu\text{m}$  vibration amplitude and 60 rpm work material rotation. The micro-hole profiles get improved with the aid of vibration and rotational effect. The better replenishment of the electrolyte and debris removal from the drilling area produces the stable and uniform gas film formation. When ultrasonic vibrations were applied to the tool electrode, they induce cyclic oscillations at a high frequency (20–30 kHz). These oscillations create rapid compressions and rarefactions in the electrolyte near the tool, enhancing electrolyte circulation and promoting faster bubble detachment. As a result, the gas film thickness is reduced, leading to a more uniform and stable gas layer. The agitation effect of ultrasonic vibrations prevents excessive clustering of hydrogen bubbles around the tool tip. Instead of forming a thick, unstable gas layer that could hinder spark initiation, the vibrations ensure continuous renewal of the film, maintaining a thin dielectric barrier that supports controlled and localized sparking. As a result, consistent sparks are produced, thereby generating better micro-holes geometries. This enhances material removal efficiency and reduces stray discharges, leading to improved machining precision.

An improvement in the micro-hole circularity is observed with tool vibrations as ultrasonic oscillations enhance electrolyte circulation, ensuring a thin and stable gas film that promotes uniform sparking and controlled material removal. Additionally, the workpiece rotational effect further aids circularity by whirling the electrolyte, preventing localized heating and facilitating even flushing of debris, reducing irregularities. The combined effect minimizes overcut variations, leading to smoother and more precise hole geometry. The developed UR-ECDD process is capable of machining other materials as well such as Quartz glass material, polymer composite material etc.

### Machining conditions and procedure

Response indicators were recorded after each run of the experiments, which are methodically designed and carried out using Taguchi's L16 orthogonal design. Taguchi's research on orthogonal arrays is a systematic method for designing trials, allowing for the investigation of multiple control parameters and their interactions. The ZEISS Stemi 508 stereo zoom microscope is used to analyse the machined micro-holes in order to examine the HOC, CE and thermal fractures. The reproducibility of the experimental setup and results is performed during the initial machining. Three experiments are performed at each of the machining conditions in order to check the variations. A total of 9 experiments is performed and repeated three times at different machining conditions. The obtained variation in each of the experimental results is within the acceptable range<sup>32</sup>. The level of the each of the parameters is selected on the basis of initial machining and literature study. This range of input parameters are preferred by various authors owing to attainment of better responses in the process<sup>33,34</sup>.



**Fig. 2.** Comparative analysis of the micro-hole geometries at 40 V, 10 wt% NaOH, 0.8 mm/min, 6  $\mu\text{m}$  and 60 rpm obtained with conventional ECDD (a & b) and with UR-ECDD (c & d). HAZ and Thermal Cracks (e) Zoomed view of the edges.

Control variables						Fixed variables	
Levels	Units	I	II	III	IV		
A: Tool vibrations (TV)	μm	3	4	5	6	Secondary tool	Graphite
B: Tool Feed Rate (TFR)	mm/min	0.6	0.7	0.8	0.9	Electrolyte	NaOH
C: Work material rotation (WR)	rpm	40	60	80	100	Primary tool	Tungsten Carbide (Dia:0.35 mm)
D: Applied Voltage (AV)	V	35	40	45	50	ECDD time	2 min
E: Electrolyte Concentration (EC)	wt%	10	15	20	25	Electrolyte above the material	1 mm

**Table 1.** Control variables and their levels utilized during UR-ECDD optimization investigation.

Typical mechanical, thermal and electrical properties of soda-lime glass	
Property	Value
Mohs hardness	6
Specific heat, $C_p$ (J/kg K)	670
Thermal conductivity, $k$ (W/m K)	1.6
Young's modulus (GPa)	68–72
Melting temperature, $T_m$ (K)	1673
Density, $\rho$ (kg/m <sup>3</sup> )	2170

**Table 2.** Critical properties of soda lime glass materials<sup>37,38</sup>.

To determine the influence of control variables, the experimental data are further examined using the signal-to-noise ratio (S/N). Then grey relational analysis (GRA) was used to do multi-criteria optimization. The control variables used in the present investigation along with their levels is given in Table 1. Soda lime glass is used as a work material in the present study, The critical properties of the soda lime glass material is given in Table 2. NaOH electrolyte remove material much faster than other electrolytes because it produces negatively charged hydroxides (OH<sup>-</sup>) required in a chemical etching of the work-piece when dissolute in water<sup>12,35</sup>. NaOH has a high electrical conductivity, which makes it easier for the electrolyte to flow current efficiently. It is critical in forming the gas film around the tool in order to produce sparks that causes the removal of material<sup>36</sup>. Figure 3 shows the time line and process flow chart of the present study procedure. The measured responses during multi-criteria optimization are listed in Table 3. All measurements of MRR, HOC and CE are repeated three times and their average value was considered as response. The standard deviation for MRR, HOC and CE is 0.12, 0.017 and 0.029 respectively.

## Measurements

Following the creation of micro-holes, measurements of the working material are carried out to perform the multi-criteria optimization. All measurements of MRR, HOC and CE are repeated three times and their average value was considered as response. Three measurements are averaged to reduce computational mistakes. However, the variation among the difference of the values is within acceptable range. For the measurement, a weighing machine (Model: CAY220, Make: CAS company) with a resolution of 0.0001 g is utilised. The micro-holes are analyzed from the hole entry side using ZEISS Stemi 508 stereo zoom microscope equipped with software to assess the HOC and CE.

## MRR

The difference in the weight of the soda lime glass working material before and after UR-ECDD process in a unit of time is used to compute the MRR.

The following is the MRR formula as given in Eq. 1:

$$\text{MRR} = ((w_{h1} - w_{h2}) / t) \quad (1)$$

where  $w_{h1}$  = weight before UR-ECDD process and  $w_{h2}$  = weight after UR-ECDD process.

## HOC

The difference between the tool diameter ( $d$ ) and the measured diameter of the hole entry ( $D_{ent}$ ) is known as hole overcut as expressed in Eq. 2. Figure 4a depicts an example of HOC during the ECDD process.

$$\text{HOC} = (D_1 - D_2) \quad (2)$$

## CE

Out of roundness error is referred to as circularity error. It is calculated as the difference between the greatest and lowest radius of the hole, as illustrated in Fig. 4b and Eq. 3, and is used to assess the circularity, or geometric correctness, of the hole<sup>11,39</sup>.

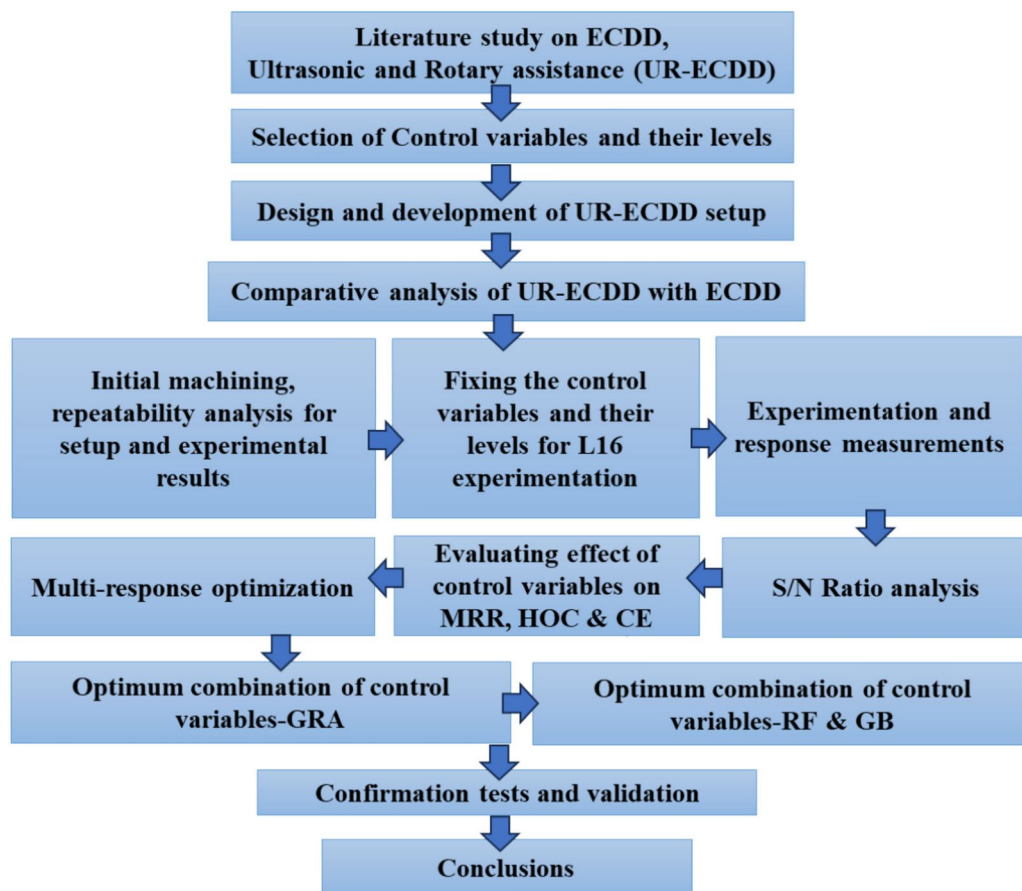
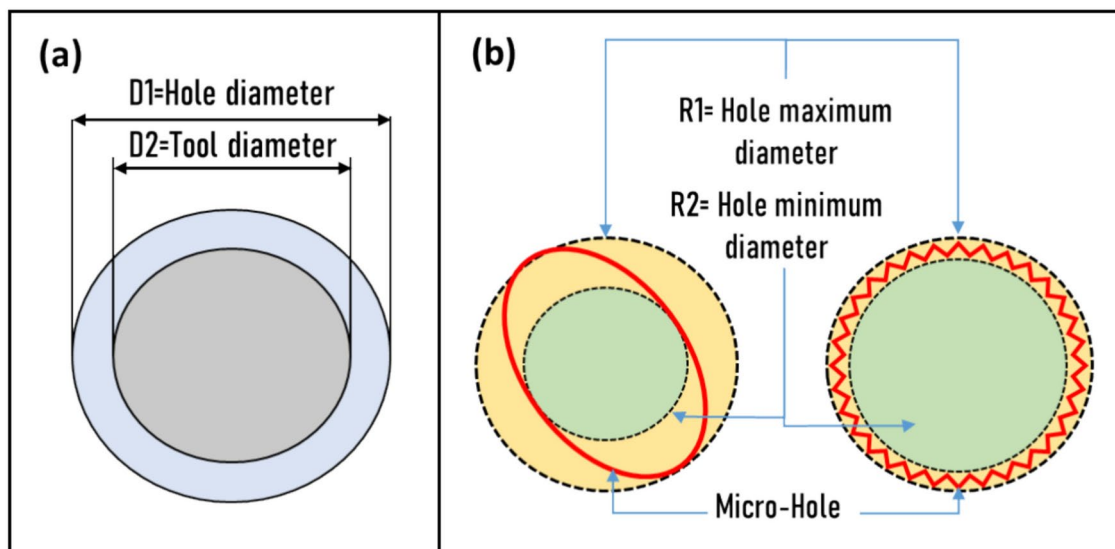


Fig. 3. Time line and process flow chart of present study.

Exp	TV ( $\mu\text{m}$ )	TFR (mm/min)	WR (rpm)	AV (V)	EC (wt%)	MRR ( $\text{mm}^3/\text{min}$ )	HOC (mm)	CE (mm)
1	3	0.6	40	35	10	0.9652	0.2354	0.1875
2	3	0.7	60	40	15	0.9564	0.2262	0.1969
3	3	0.8	80	45	20	0.9616	0.2135	0.2078
4	3	0.9	100	50	25	0.9452	0.2351	0.2251
5	4	0.6	60	45	25	1.1858	0.2124	0.1730
6	4	0.7	40	50	20	1.1649	0.2084	0.2021
7	4	0.8	100	35	15	1.1585	0.2184	0.1976
8	4	0.9	80	40	10	1.1887	0.1912	0.1799
9	5	0.6	80	50	15	1.2185	0.2041	0.1598
10	5	0.7	100	45	10	1.2187	0.2090	0.1787
11	5	0.8	40	40	25	1.2115	0.1887	0.1612
12	5	0.9	60	35	20	1.2015	0.1864	0.1387
13	6	0.6	100	40	20	1.2458	0.2115	0.1378
14	6	0.7	80	35	25	1.2618	0.1923	0.1354
15	6	0.8	60	50	10	1.2213	0.1918	0.1428
16	6	0.9	40	45	15	1.2215	0.1798	0.1337

Table 3. Observed responses in present UR-ECDD optimization investigation.



**Fig. 4.** Measurement technique for (a) HOC (b) CE<sup>11,39,40</sup>.

Exp	TV ( $\mu\text{m}$ )	TFR (mm/min)	WR (rpm)	AV (V)	EC (wt%)	MRR ( $\text{mm}^3/\text{min}$ )	HOC (mm)	CE (mm)
1	1	1	1	1	1	- 0.30765	12.5639	14.5400
2	1	2	2	2	2	- 0.38721	12.9101	14.1151
3	1	3	3	3	3	- 0.34011	13.4120	13.6471
4	1	4	4	4	4	- 0.48953	12.5749	12.9525
5	2	1	2	3	4	1.48023	13.4569	15.2391
6	2	2	1	4	3	1.32577	13.6220	13.8887
7	2	3	4	1	2	1.27792	13.2149	14.0843
8	2	4	3	2	1	1.50145	14.3702	14.8994
9	3	1	3	4	2	1.71651	13.8031	15.9285
10	3	2	4	3	1	1.71794	13.5971	14.9575
11	3	3	1	2	4	1.66647	14.4846	15.8527
12	3	4	2	1	3	1.59448	14.5911	17.1585
13	4	1	4	2	3	1.90897	13.4938	17.2150
14	4	2	3	1	4	2.01981	14.3204	17.3676
15	4	3	2	4	1	1.73645	14.3430	16.9054
16	4	4	1	3	2	1.73787	14.9042	17.4774

**Table 4.** Experiment runs and their computed S/N ratios.

$$CE = (R_1 - R_2) \quad (3)$$

### Consent to publish

All authors have read and approved this manuscript.

### Results analysis and findings

#### Signal to noise ratio analysis

S/N analysis entails evaluating the individual parametric combinations of input variables for all measured responses, as shown in Table 4. S/N ratios for responses with a "higher-the-better" target, such as MRR are calculated as follows:

$$S/N = -10 \log_{10} \left[ \frac{1}{n} \sum_{i=1}^n \left( \frac{1}{MRR_i} \right)^2 \right] \quad (4)$$

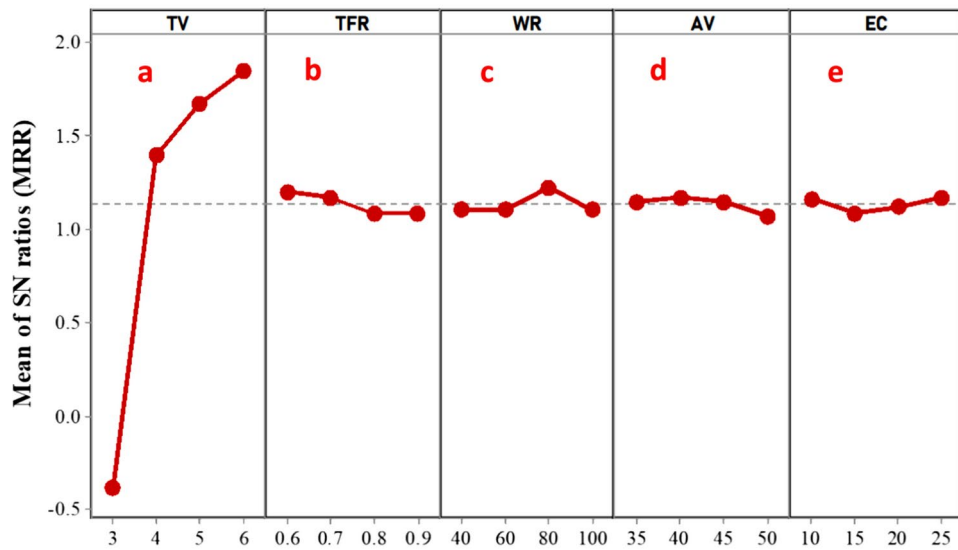
On the other hand, when calculating the S/N ratio for responses with a "smaller-the-better" objective, such as HOC and CE, the expression is as follows:

S/N ratio mean of MRR						S/N ratio mean of HOC				
Level	TV (μm)	TFR (mm/min)	WR (rpm)	AV (V)	EC (wt%)	TV (μm)	TFR (mm/min)	WR (rpm)	AV (V)	EC (wt%)
1	-0.3811	<b><i>1.1995</i></b>	1.1056	1.1461	1.1620	12.87	13.33	13.89	13.67	13.72
2	1.3963	1.1691	1.1060	<b><i>1.1724</i></b>	1.0863	13.67	13.61	13.83	13.81	13.71
3	1.6738	1.0852	<b><i>1.2244</i></b>	1.1490	1.1223	14.12	13.86	<b><i>13.98</i></b>	<b><i>13.84</i></b>	<b><i>13.78</i></b>
4	<b><i>1.8508</i></b>	1.0861	1.1038	1.0723	<b><i>1.1692</i></b>	<b><i>14.27</i></b>	<b><i>14.11</i></b>	13.22	13.59	13.71
Delta	2.2319	0.1143	0.1206	0.1001	0.0830	1.40	0.78	0.76	0.26	0.07
Rank	<b>1</b>	<b>3</b>	<b>2</b>	<b>4</b>	<b>5</b>	<b>1</b>	<b>2</b>	<b>3</b>	<b>4</b>	<b>5</b>

S/N ratio mean of CE										
Level	TV (μm)	TFR (mm/min)	WR (rpm)	AV (V)	EC (wt%)					
1	13.81	<b><i>15.73</i></b>	15.44	<b><i>15.79</i></b>	15.33					
2	14.53	15.08	<b><i>15.85</i></b>	15.52	15.40					
3	15.97	15.12	15.46	15.33	<b><i>15.48</i></b>					
4	<b><i>17.24</i></b>	15.62	14.80	14.92	15.35					
Delta	3.43	0.65	1.05	0.87	0.15					
Rank	<b>1</b>	<b>4</b>	<b>2</b>	<b>3</b>	<b>5</b>					

**Table 5.** Rank and delta value of response indicators. Significant values are in (bold/italics).



Signal-to-noise: Larger is better

**Fig. 5.** MRR mean of SN ratio, (a) TV, (b). TFR, (c). WR, (d). AV, and (e). EC.

$$S/N = -10 \log_{10} \left[ \frac{1}{n} \sum_{i=1}^n ((HOC \text{ or } CE)_i)^2 \right] \tag{5}$$

In this case, 'n' denotes the number of measurements, and 'i' represents the response. A greater magnitude of the S/N ratio is typically viewed as reflecting the most significant variable in obtaining the desired results. The mean of the S/N ratio and the delta value are used in this investigation to find the best combination of input variables (Table 5). The delta value is calculated as the difference between the response lowest and highest mean values<sup>11,41</sup>.

*Analysis of control variables impacting MRR*

In Fig. 5, the main effects plot visually communicates the relationship between the Signal-to-Noise (S/N) ratio and MRR. Table 5, provides delta values for the MRR response and in compliance with Fig. 5. These delta values represent the differences between the lowest and highest mean values, offering insights into the variations in MRR across different experimental conditions. It is observed that MRR is highly influenced by the TV (Rank 1, 2.2319) followed by WR (Rank 4, 0.1206), TFR (Rank 3, 0.1143), AV (Rank 4, 0.1001), and lastly by EC (Rank 5, 0.0830). Figure 6 shows the contour plot of the MRR with respect to different control variables. The optimum

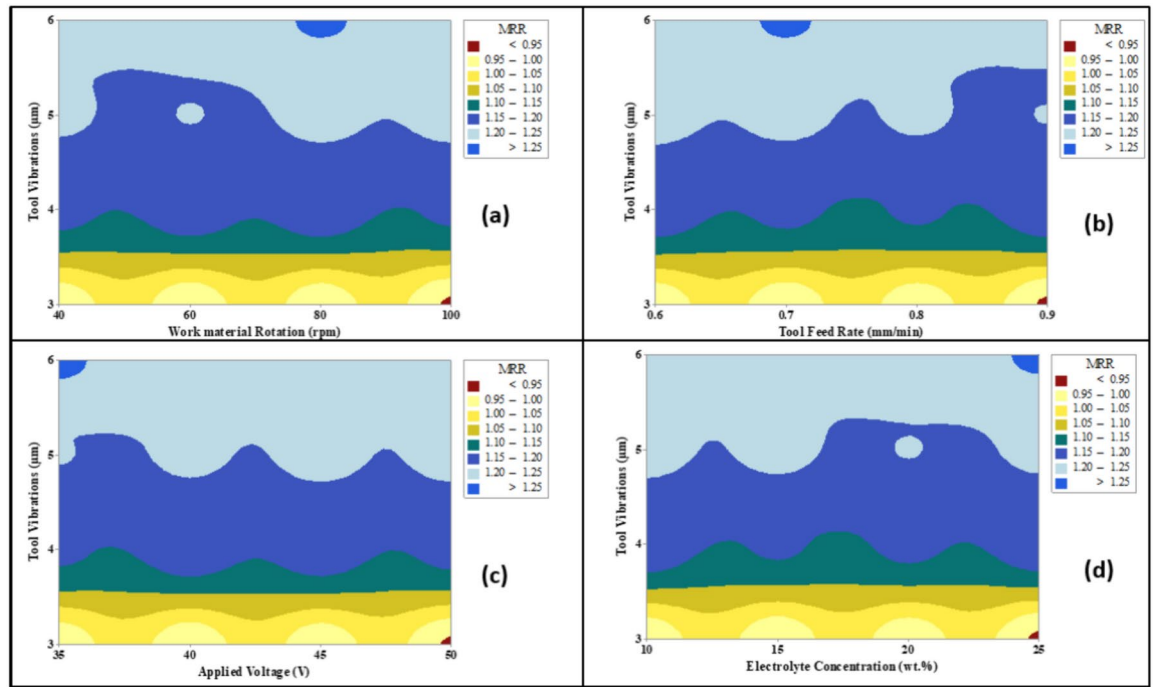


Fig. 6. MRR contour plot at different control variables (a) TV & WR (b) TV & TFR (c) TV & AV (d) TV & EC.

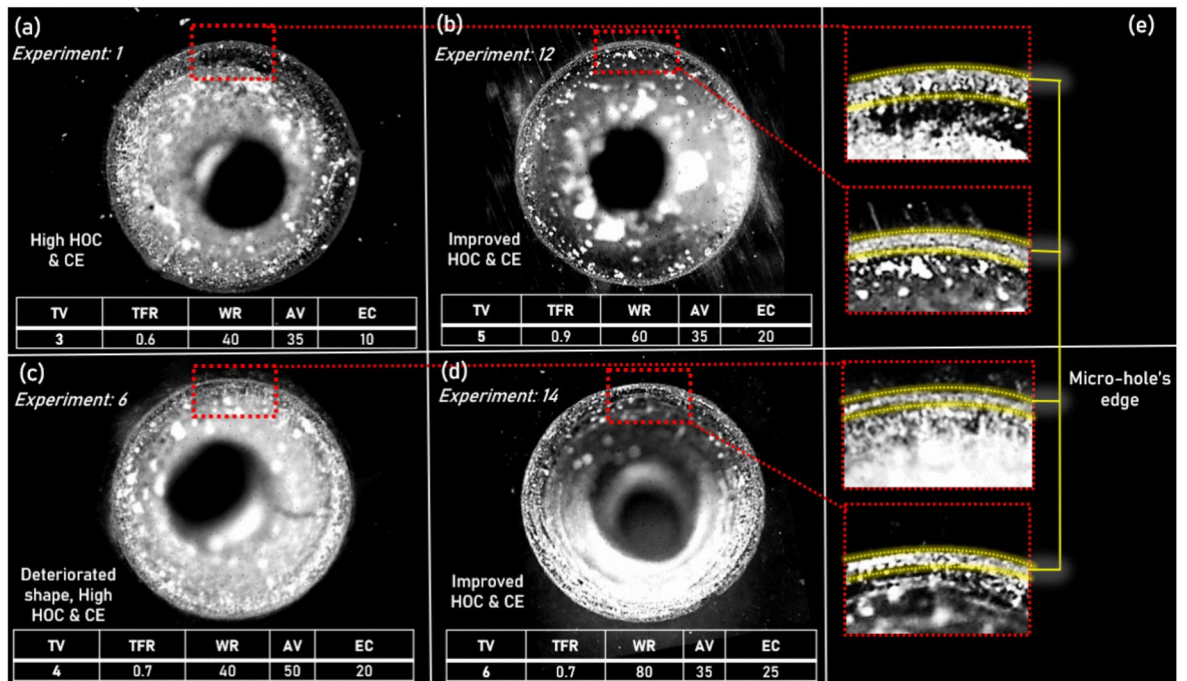


Fig. 7. Microscopy images of the drilled micro-holes produced at different control variables using UR-ECDD process.

setting of control variables combination for maximizing MRR is A4C3B1D2E4, corresponding to (3 µm, 80 rpm, 0.6 mm/min, 40 V, 25 wt%).

Tool vibrations (TV) help in attaining the thin gas layer airing the tool that enhances the spark uniformity and as a result, improved MRR is obtained. An increase in TV results into an increase in MRR owing to have better and consistent flow of the electrolyte in the drilling area. A significant improvement of 29% in the MRR is noticed with the increase of TV from 3 to 6 µm as seen from Figs. 5 and 6 (Table 2, Experiments 1&13). Figure 7

shows the microscopy images of the micro-holes drilled with the UR-ECDD process. An increase of MRR is visible in Figs. 5a and 6, with the increase of TV from 3 to 5  $\mu\text{m}$  (Table 2, Experiments 1&12).

It is further illustrated that as the rotational speed of the work material increases, there is an increase in the MRR because the rotary motion helps the drilling of micro holes with better machining depth<sup>34</sup>. It also improves electrolyte circulation between the tool and the working material. This method has a significant benefit in that the energy from the spark is distributed uniformly over the whole drilling area, resulting in straight and clean-cut holes. Additionally, at a very high WR, MRR tends to decrease because of splashing of the electrolyte, which then cause a hindrance in the formation of the gas layer (Figs. 5b, 6a). An increase of 0.0403  $\text{mm}^3/\text{min}$  in MRR is calculated with the increase of WR from 40 to 80 rpm at 6  $\mu\text{m}$  TV. Figure 7d shows the improvement in MRR in comparison to Fig. 7a due to the increase in WR from 40 to 80 rpm (Experiments 1 & 14).

Tool feed rate plays a significant role in MRR (Fig. 5c & Table 5). Increasing the tool feed rate tends to decrease the MRR, as higher tool feed rates result in less interaction between the tool and the work material, leading to reduced thermal energy within the drilling area. As a result, low MRR is obtained at higher TWR. Figure 6b shows the increase in MRR with the decrease of TFR from 0.9 to 0.6  $\text{mm}/\text{min}$ . It shows that the area having higher value of MRR exists at the lower values of the TFR.

The performance of MRR improves noticeably as applied voltage increases (Figs. 5d, 6c). This improvement can be due to the fact that higher voltage levels cause a greater number of hydrogen bubbles to form at the tool-electrolyte interface. This increases the rate at which a gas layer forms, resulting in high-intensity sparks over the soda lime glass substance. As the concentration of the electrolyte increases, the MRR increases (Figs. 5e, 6d). Increased electrolyte concentration facilitates fast electrochemical reactions due to the speedy dissociation of  $\text{H}^+$  and  $\text{OH}^-$  in the electrolytic solution. This causes the gas layer surrounding the tool to form quicker. It increases MRR by increasing spark striking and producing enormous heat in the drilling area.

**Analysis of control variables impacting HOC** HOC is defined as the additional material removed in comparison to the tool diameter and is calculated using Eq. 3 (Fig. 4). Figure 8 illustrates the main effect plot of OC while Fig. 9 presents the contour plot of the MRR with respect to control variables. This figure provides a graphical representation of how HOC varies with the increase and decrease in control variables.

Analyzing the delta values of HOC in Table 5, reveals a substantial influence of TV on HOC, ranking highest at 1.40 (Rank 1), followed by TFR at 0.78 (Rank 2), WR at 0.76 (Rank 3), AV at 0.26 (Rank 4) and electrolyte concentration at 0.07 (Rank 5). The optimum setting of control variables combination for minimizing HOC is A4B4C3D3E3, corresponding to (6  $\mu\text{m}$ , 0.9  $\text{mm}/\text{min}$ , 45 V, 20 wt%). A significant improvement of 20.81% in the HOC is noticed with the increase of TV from 3 to 5  $\mu\text{m}$  as seen from Figs. 6 and 7 (Table 2, Experiments 1&12). An improvement in HOC is visible in microscopy images of the micro-holes (Fig. 7a, b), with the increase of TV from 3 to 5  $\mu\text{m}$ .

At higher TFR, OC tends to decrease because of the reduced contact between the tool and the work material. Less thermal energy is transmitted in the drilling area as a result. As expected, heat energy transmission by sparks decreases with increasing TFR, improving HOC (Fig. 9b). At a constant TV of 4  $\mu\text{m}$ , the HOC drops 11% when the TFR level is changed from 0.6 to 0.9  $\text{mm}/\text{min}$  (Experiments 5 & 8).

Further, HOC improves with the increase in WR since the rotational effect improves the electrolyte replenishment in the drilling area and hence, better sparks consistency around the tool. The occurrence of the spray sparks that causes an increase in overcut decreases with the application of the WR. An improvement of 22.4% in HOC is calculated with the increase of WR from 40 to 80 rpm at 6  $\mu\text{m}$  TV. Figure 7d shows the

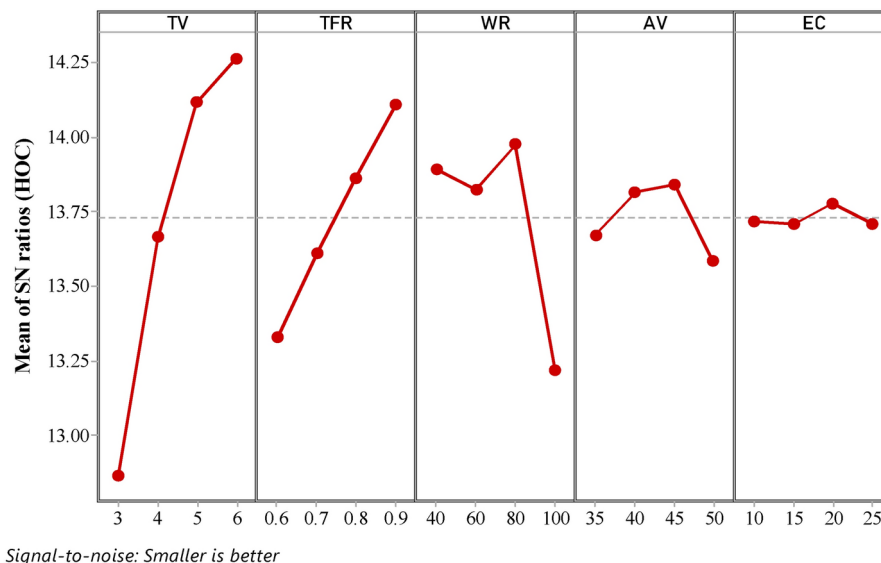


**Fig. 8.** HOC mean of SN ratio.

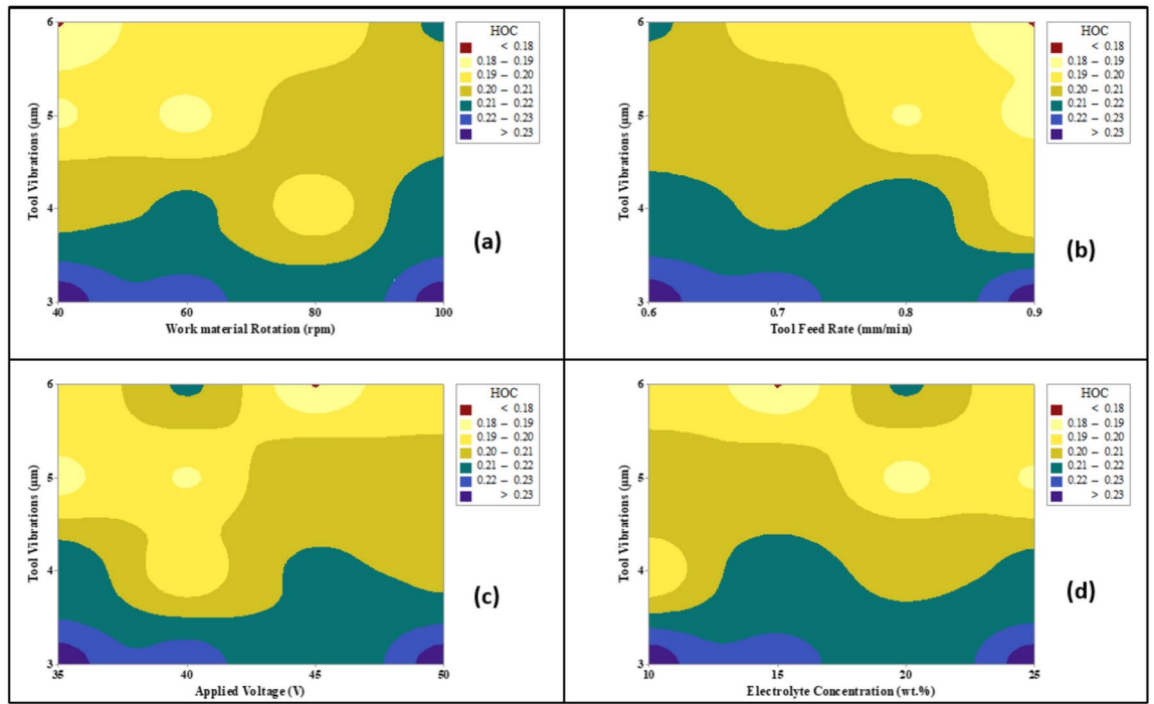
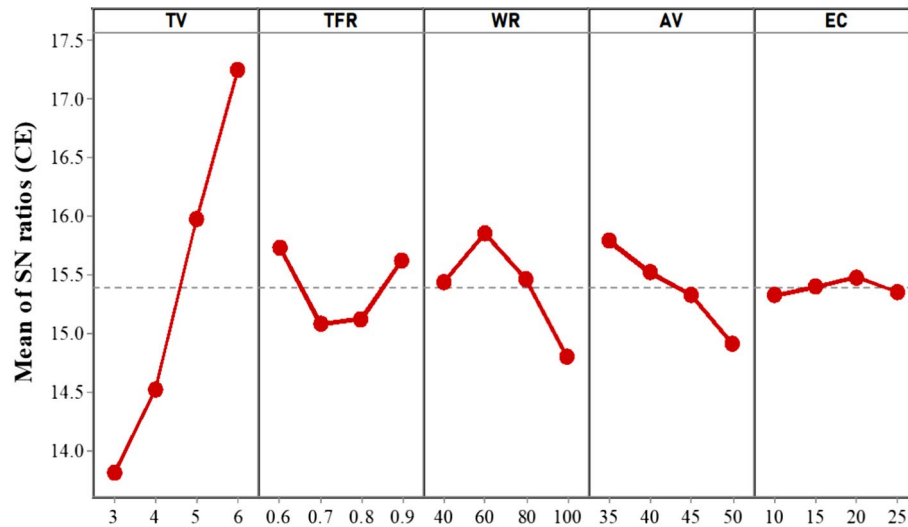


Fig. 9. HOC contour plot at different control variables (a) TV & WR (b) TV & TFR (c) TV & AV (d) TV & EC.



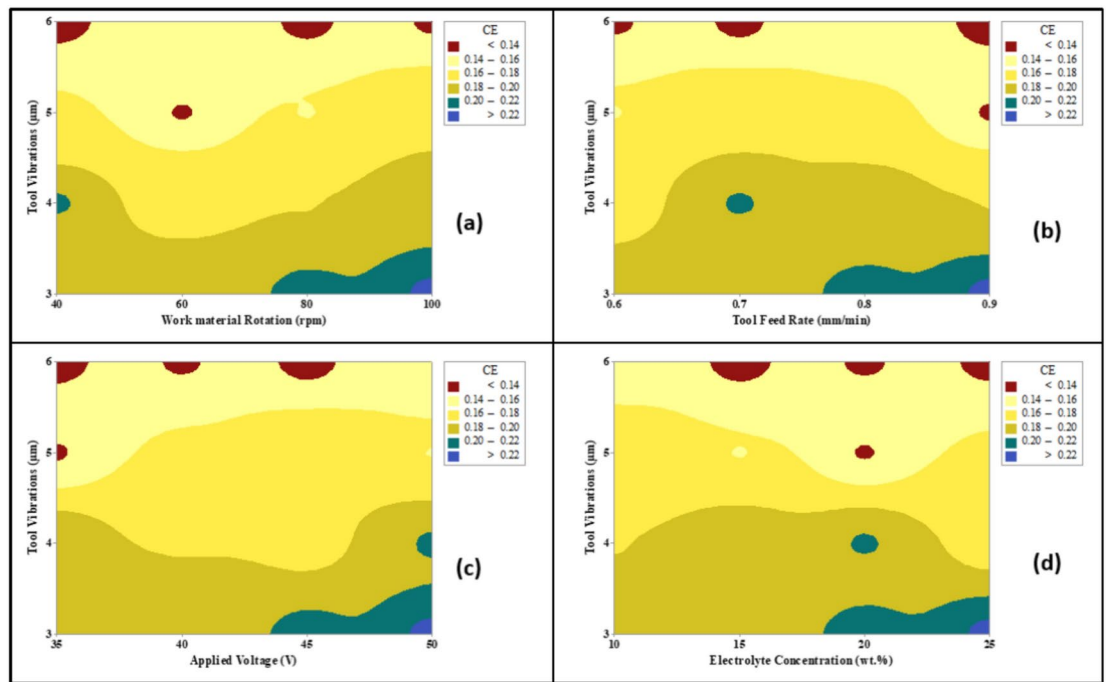
Signal-to-noise: Smaller is better

Fig. 10. HOC mean of SN ratio.

improvement in MRR in comparison to Fig. 7a due to the increase in WR from 40 to 80 rpm (Experiments 1 & 14).

Higher applied voltage and electrolyte concentration lead to deterioration of HOC due to increased bubble formation intensity, spark frequency, and chemical action at the micro-hole edge. This enlargement occurs due to increased heat energy transfer from the tool tip in the drilling area, resulting in a higher HOC. Notably, a performance improvement of 11.3% in HOC is noted with a concentration decrease from 25 wt% to 10 wt% and an applied voltage decrease from 45 to 40 V (Experiment 5 & 8, Figs. 8 and 9, Table 2).

**Analysis of control variables impacting CE** CE is described as the out of roundness error or its deviation from a circular shape, and is calculated using Eq. 3 (Fig. 4). Figure 10 shows the CE main effect plot, whereas Fig. 11 shows a contour plot indicating how CE evolves in relation to the control values. The delta values as given in



**Fig. 11.** HOC contour plot at different control variables (a) TV & WR (b) TV & TFR (c) TV& AV (d) TV & EC.

Table 5 reveals that TV has a significant effect on CE (Rank 1, 3.43) followed by the WR (Rank 2, 1.05), AV (Rank 3, 0.87), TFR (Rank 4, 0.65) and EC (Rank 5, 0.15). The optimal combination of control variables for minimizing CE is A4C2D1B1E3 corresponding to (6  $\mu\text{m}$ , 80 rpm, 35 V, 0.6 mm/min, 20 wt%). Notably, increasing TV from 3 to 6  $\mu\text{m}$  results in a significant 36.06% improvement in CE, as observed in Figs. 10 and 11 (Table 2, Experiments 1&13). Figure 11a–d has portrayed the HOC contour plot at different control variables.

Microscopy images in Fig. 7a, b further confirm the improved CE with a TV increase from 3 to 5  $\mu\text{m}$ . The adequate availability of the electrolyte in the drilling area leads to the uniform and stable gas layer formation. As a result, consistent sparks take place at the tool periphery which further leads to the improvement of the CE.

Furthermore, an increase in WR improves the CE because the rotating impact improves electrolyte replenishment in the drilling region, resulting in more constant sparks around the tool. With the application of WR, the incidence of stray sparks that tends to produce irregular shape of the micro-holes is reduced. When the WR is raised from 40 to 80 rpm at a TV of 6  $\mu\text{m}$ , the CE improves by 38.47%. Figure 7d illustrates this, with better CE compared to Fig. 7a due to greater WR (Experiments 1 & 14).

AV significantly impacts TFR by controlling spark intensity over the working material, which increases with applied voltage, leading to an increase in CE. AV minimizes stray sparks from the tool, influencing roundness error and other control variables.

Higher TFR leads to decreased OC due to reduced tool and work material contact, resulting in less thermal energy transfer in the drilling area. As expected, CE improves with increasing TFR since the transference of the heat energy through the sparks decreases (Fig. 11b). When TFR is adjusted from 0.6 to 0.9 mm/min, CE decreases by 11% at a constant TV of 4  $\mu\text{m}$  (Experiments 5 & 8).

Higher electrolyte concentration deteriorates the CE due to increased bubble formation intensity, spark frequency at the tungsten tool tip, and enhanced chemical action at the micro-hole edge. Notably, a performance improvement of 16.7% in CE is observed with a decrease in concentration from 25 to 10 wt% and a reduction in applied voltage from 50 to 35 V (Experiments 1 & 4, Tables 2 and 4).

### Multi-criteria response optimization

MRR, HOC and CE are response factors that are sensitive to changes in input components. According to the S/N Ratio investigation, the maximum MRR is produced at high level of TV, third level of WR, low level of TFR, second level of applied voltage and high level of EC i.e., A4C3B1D2E4, corresponding to 3  $\mu\text{m}$ , 80 rpm, 0.6 mm/min, 40 V, 25 wt%. The optimal value of control variables for HOC is determined as high level of both TV & TFR while third level of WR, AV & EC i.e., A4B4C3D3E3, corresponding to 6  $\mu\text{m}$ , 0.9 mm/min, 45 V, 20 wt%. The optimal value of control variables for CE, on the other hand, is determined as high level of TV, second level of WR, low levels of TWR & AV, third level of EC i.e., A4C2D1B1E3 corresponding to 6  $\mu\text{m}$ , 80 rpm, 35 V, 0.6 mm/min, 20 wt%. Since, the levels of control variables are different for the different response indicators, so finding the best method combination for multi-criteria optimization is a big problem<sup>42</sup>. Hence, the multi-criteria optimization approach of Grey Relational Analysis (GRA) is utilised to identify the ideal combination to tackle this problem.

## Grey relational analysis

In the context of GRA, optimizing multi-criteria response indicators means converting it into a single-objective optimization problem. GRA consists of three steps: (i) Grey Relational Generation, (ii) Grey Relational Coefficients (GRC), and (iii) Grey Relational Grades (GRDs).

Figure 12 shows the procedure for GRA process. During the GRA, the experimental data of all response indicators are normalised using Eqs. 5 and 6, respectively. To create a comparable sequence in the 0–1 range, this normalisation is necessary<sup>7,22,25</sup>. The measured responses are classified into two categories: "higher-the-better" and "smaller-the-better." Eq. 6 is used to normalise answers that fall into the "higher-the-better" category, such as MRR, whereas Eq. 7 is used to normalise responses that fall into the "smaller-the-better" category, such as HOC & CE.

$$y_i = \frac{\max(x_i) - (x_i)}{\max(x_i) - \min(x_i)}$$

$$y_i = \frac{(x_i) - \min(x_i)}{\max(x_i) - \min(x_i)} \quad (6)$$

In the provided equations,  $y_i$  represents the normalized value,  $x_i$  is the measured response value, 'min' and 'max' denote the minimum and maximum values of  $x_i$  and  $i$  signifies the number of response sequences. The next step includes utilising Eq. 7 to calculate the GRC once the sequence has been normalised. The identification coefficient, denoted by the factor " $\beta$ " in this equation, has a value that might be between 0 and 1<sup>7,29</sup>. Each factor is given equal weight in this investigation, hence  $\beta$  is set to 0.5, a standard value in GRA. However, the selection of the weighing factors may influence the results but decision makers must choose its value before applying the GRA on the basis of their relative value for different responses in analysis.

The normalised values and associated GRCs for the response factors are provided in the Table 6.

$$\text{GRC} = N_i(k) = \frac{\Delta_{\min} + \beta\Delta_{\max}}{\Delta_i + \beta\Delta_{\max}} \quad (7)$$

where  $\Delta_i$  is the difference between the maximum and sequential response factors,  $\Delta_{\min}$  and  $\Delta_{\max}$  is the minimum and maximum value of  $\Delta_i$ . Grey Relational Grades (GRG) is obtained by considering average of GRC values as given in Eq. 8.

$$\text{GRG} = (\gamma_i) = \frac{1}{n} \sum_{k=1}^n N_i(k) \quad (8)$$

Table 6 shows the relationship between the estimated GRGs for all the input factors' combination while Table 7 presents the mean of GRG along with their corresponding ranks. According to a higher-order GRG, the results of the experiment for that grade are more likely to meet the optimum response requirements<sup>29</sup>. As a result, the GRG analysis determined that the A4B4C1D3E2 (6  $\mu\text{m}$ , 0.9 mm/min, 40 rpm, 45 V & 15 wt%) combination of optimal factors for this investigation corresponds to experiment 16. Figure 13 shows the bubble plot of the GRG obtained during the multi-objective response optimization at different tool vibrations using work material

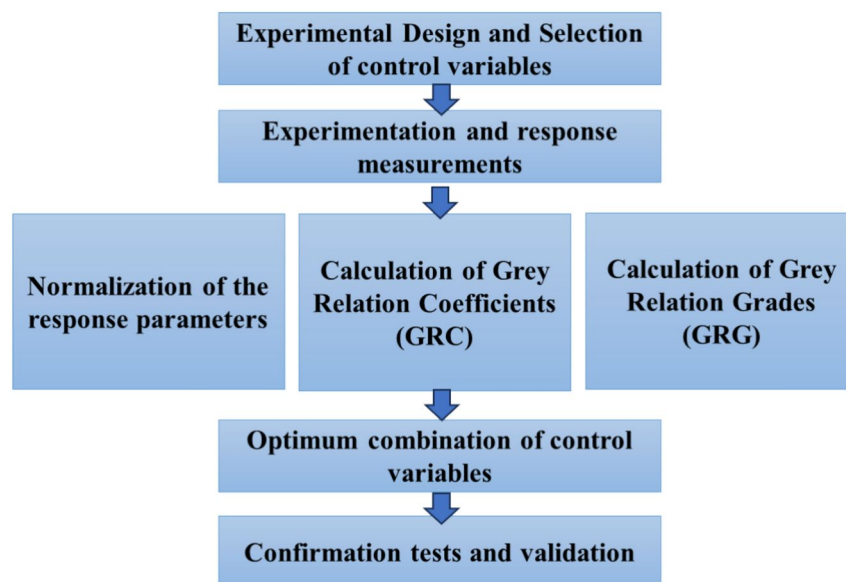


Fig. 12. Step wise procedure in the GRA.

Exp	Normalized value			GRC			GRG (grey relational grades)	
	MRR	HOC	CE	MRR	HOC	CE	Value	Order
1	0.0632	0.0000	0.4114	0.348	0.3333	0.4593	0.3802	14
2	0.0354	0.1655	0.3085	0.3414	0.3747	0.4196	0.3786	15
3	0.0518	0.3939	0.1893	0.3453	0.4520	0.3815	0.3929	13
4	0.0000	0.0054	0.0000	0.3333	0.3345	0.3333	0.3337	16
5	0.7599	0.4137	0.5700	0.6756	0.4603	0.5376	0.5578	10
6	0.6939	0.4856	0.2516	0.6203	0.4929	0.4005	0.5046	11
7	0.6737	0.3058	0.3009	0.6051	0.4187	0.4170	0.4803	12
8	0.7691	0.795	0.4945	0.6841	0.7092	0.4973	0.6302	8
9	0.8632	0.5629	0.7144	0.7852	0.5336	0.6365	0.6518	7
10	0.8639	0.4748	0.5077	0.7860	0.4877	0.5039	0.5925	9
11	0.8411	0.8399	0.6991	0.7588	0.7575	0.6243	0.7135	6
12	0.8095	0.8813	0.9453	0.7241	0.8081	0.9014	0.8112	3
13	0.9495	0.4299	0.9551	0.9083	0.4672	0.9176	0.7644	5
14	1.0000	0.7752	0.9814	1.0000	0.6898	0.9641	0.8846	2
15	0.8721	0.7842	0.9004	0.7963	0.6985	0.8339	0.7762	4
16	0.8727	1.0000	1.0000	0.7971	1.0000	1.0000	0.9324	1

Table 6. GRG values for the measured response indicators.

Level	TV ( $\mu\text{m}$ )	TFR (mm/min)	WR (rpm)	AV (V)	EC (wt%)
1	0.3714	0.58855	0.632675	<b>0.639075</b>	0.594775
2	0.5432	0.590075	0.63095	0.621675	0.610775
3	0.69225	0.590725	<b>0.639875</b>	0.6189	0.618275
4	<b>0.8394</b>	<b>0.676875</b>	0.542725	0.566575	<b>0.6224</b>
Delta	0.468	0.088325	0.09715	0.0725	0.027625
Rank	1	3	2	4	5

Table 7. Mean GRG. Significant values are in bold.

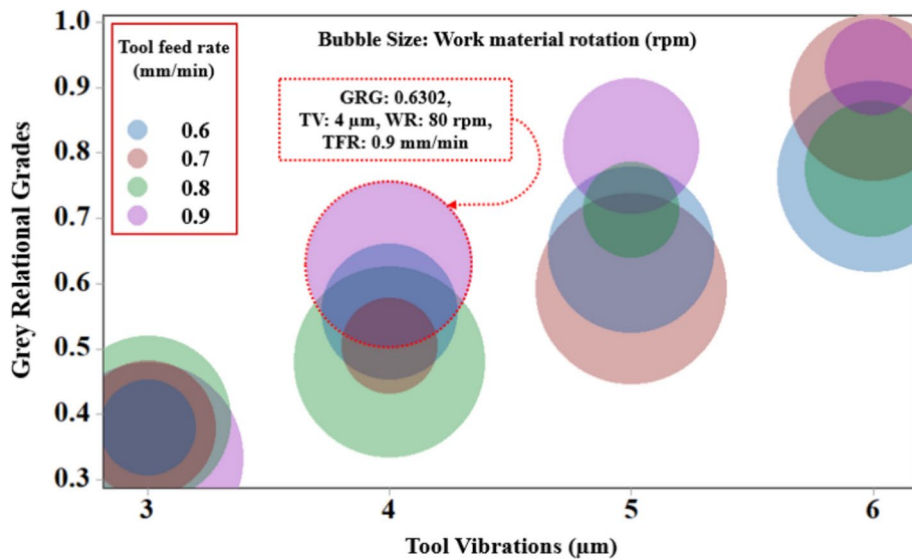


Fig. 13. Bubble plot of the GRG at different control variables.

rotation as a bubble size and tool feed rate as a categorical variable. It shows the scattering of the GRG at different input variables.

However, taking into account all four levels is crucial in order to fully comprehend the influence of each control factor on the grey relational grades. Thus, as shown in Fig. 14, the final combination of input process factors is determined using the GRG means.

The best combination for the combined response indicators i.e., maximizing MRR, minimizing HOC and minimizing CE is identified as A4C3B4D1E4 (6  $\mu\text{m}$ , 80 rpm, 0.9 mm/min, 35 V, 25 wt%) using the delta ranking technique. The results show that the tool vibrations have the maximum effect on the multi-criteria response indicators followed by the rotational effect, tool feed rate, applied voltage and electrolyte concentration. Higher level of tool vibrations results in the faster replenishment of the electrolyte that produce uniform and consistent sparks within the drilling region. Third level of work material rotation results into the stable formation of the gas layer and as a result, better spark uniformity around the tool is observed. Additionally, the sludge is easily removed from the drilling region owing to centrifugal forces developed through rotational effect.

Because there is less contact between the tool and soda lime glass, the impact of the heat energy from the spark decreases in the drilling zone at a high tool feed rate. Higher tool feed rates are hence advantageous for lowering low HOC and preferred MRR. The low level of applied voltage is necessary to the reduced HOC & CE with the generation of the low intensity sparks since high level of applied voltage tends to result in higher HOC & CE due to increase in spark intensity. As a result, low level applied voltage results in improved HOC & CE with preferable MRR. The response indicators during multi-criteria optimization are least affected by the electrolyte concentration (Rank 5), its higher level tends to produce necessary sparks required for the removal of the material and etching action around the hole periphery.

### GRA-confirmation test

Confirmation tests must be performed in order to verify the enhancement of the response variables at the identified level. The GRG is predicted using Eq. 9.

$$G = G_m + \sum_{i=1}^j (G_i - G_m) \quad (9)$$

where  $G_i$  is the mean GRG at the optimal level of factors,  $G$  is the anticipated GRG,  $j$  is the number of control factors, and  $G_m$  is the overall mean GRG. GRG as a whole is 0.6115.

When the control factors are at their optimum levels (A4C3B4D1E4), the calculated GRG is found to be 0.8864. The outcomes of the confirmation test performed at these optimum levels are shown in Table 8. A total of three experiments repetitively at same optimized conditions is performed and the obtained variation is within the acceptable range. The results of the confirmation tests, which are determined by averaging three trials, closely resemble the predictions made through GRGs. Interestingly, there has been a 42.16% improvement in the GRG between the initial condition (A2B2C2D2E2) and the optimal conditions (A4C3B4D1E4).

A set of microscopic pictures showing the micro-holes drilled using the optimized input factors as well as the initial input factors are shown in Fig. 15. A visual comparison of these two picture sets shows significant improvements in all the response indicators alongside the improvement in the HAZ and thermal cracks of the micro-holes. When the holes are made using the optimised input factors, this improvement is quite noticeable. The implementation of these optimised input variables is a critical component of the drilling process for attaining

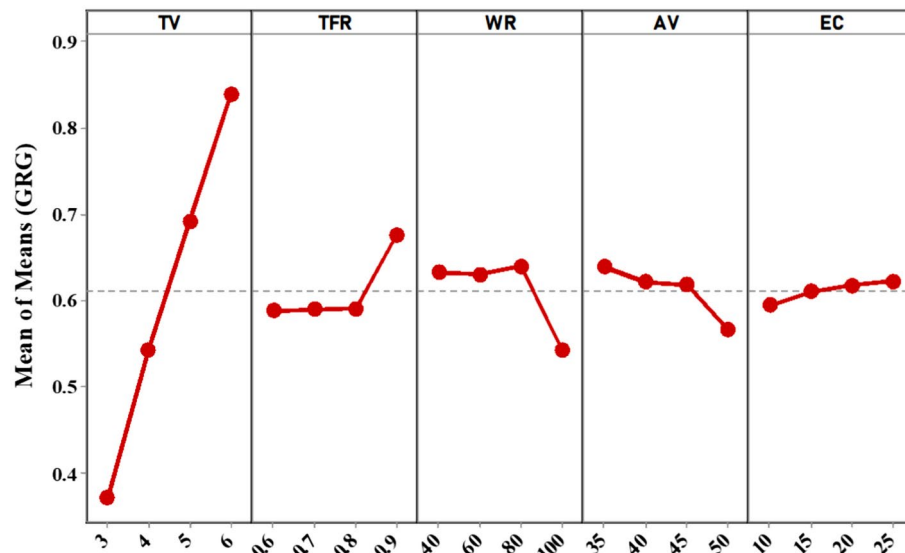
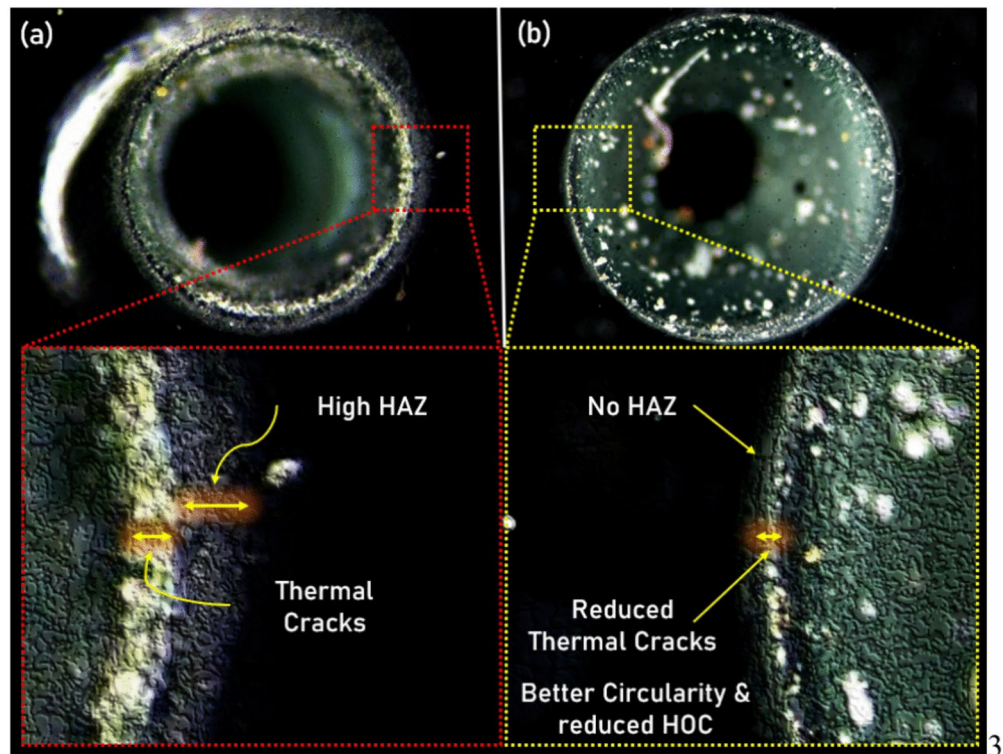


Fig. 14. Mean plot of GRG.

Levels of control factors		GRG values
Initial input control factors (A2B2C2D2E2)		0.5934
Optimum levels of input factors (A4C3B4D1E4)	Predicted	0.8243
	Experimental	0.8436

**Table 8.** Confirmation tests at the optimum level of control variables.



**Fig. 15.** Confirmation test: microscopy images of the micro-holes (a) Initial machining conditions (b) Optimum machining conditions (GRA).

superior outcomes, since the reduction of the HOC, CE, HAZ and the mitigation of thermal fractures are critical to guaranteeing the high-quality and integrity of the end product.

### Machine learning approach

Machine learning (ML) contributes an essential part in optimizing the machining process. It supports real-time process control, predictive maintenance, material characterisation, parameter optimisation, anomaly detection, and quality prediction. ML can identify the best parameter settings, manage the process in real-time, forecast maintenance requirements, evaluate the quality of the machined workpiece, identify anomalies, and direct the selection of parameters for various materials by examining data from previous machining operations.

### Gradient boost regression

The use of Gradient Boosting Regression is a machine learning technique that can be applied to regression problems<sup>43</sup>. The process involves adding more predictions to the overall system, with each one improving on the previous one. By training various models and combining their predictions to create a final prediction, this method of ensemble learning is employed. Gradient Boosting usually uses decision trees as core learners, often called “weak learners” because they are simple models<sup>44</sup>. Sequential training: It trains several models iteratively. Each new model tries to correct the mistakes made by the previous one. It uses a technique called gradient descent to minimize the loss function. At each iteration, it calculates the gradient of the loss function against the output of the ensemble and then updates the ensemble in the direction that minimizes the loss<sup>45</sup>.

The origin of the boosting approach is actually a response<sup>46</sup> to Kearns’s question: is one strong student equal to a group of weak learners? A strong base model is a more accurate prediction or classification algorithm that is arbitrarily highly correlated with the problem; a weak learner is an algorithm that performs just marginally better than random guessing. The response to this query is crucial. When estimating a weak model, it is frequently simpler than estimating a strong model. Schapire<sup>46</sup> demonstrates that the answer is yes by combining many weak models into a single, very accurate model using boosting methods.

Boosting is a method of building base models sequentially to improve prediction accuracy. Iteratively building multiple models, focusing on challenging instances, is the key difference between bagging and boosting. Bagging involves uniformly selecting each sample to construct the training dataset, while boosting strategically adjusts the distribution of training data at each step, focusing on previously misclassified or inaccurately estimated samples. This approach assigns higher weights to misclassified samples, giving them greater prominence in subsequent training iterations. The goal is to rectify the errors of previous models<sup>47,48</sup>.

### Random forest regression

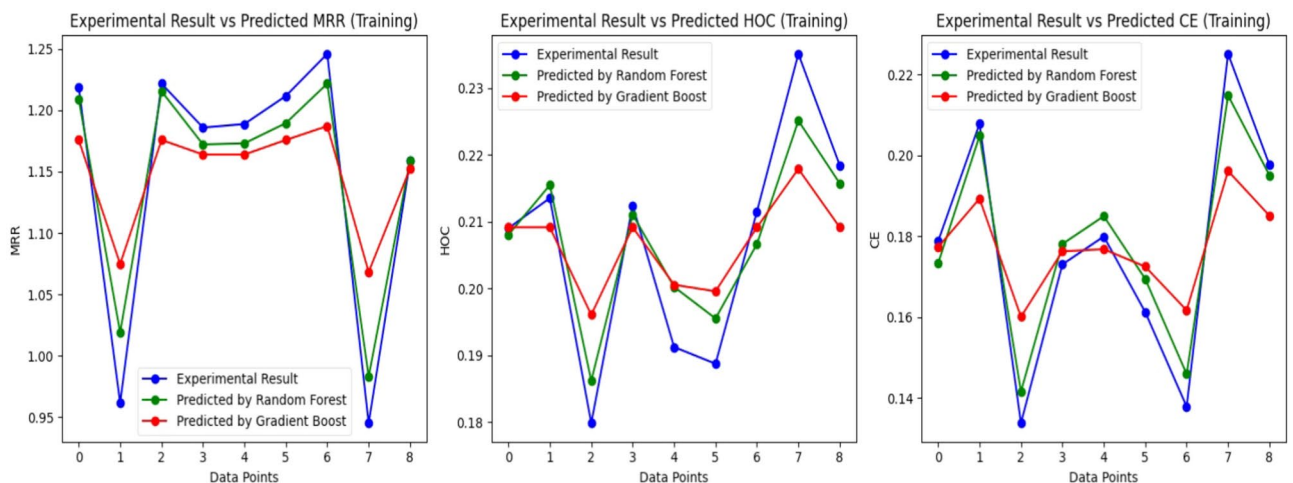
A supervised machine learning prediction method built using decision tree algorithms is called random forest regression (RFR)<sup>49</sup>. It is a model ensemble approach that builds model aggregations and lowers the costs of storing, training, and drawing conclusions from several models, all while improving test accuracy. One of the well-known ensemble techniques for regression is random forest. The random forest's output is the average of each prediction tree as this ensemble technique trains a large number of decision trees—hence the name "forest." It is predicated on the random subspace and bagging technique. The main idea behind bagging, or bootstrapping, is to train every learner using a distinct set of data. A random forest has several trees planted in it<sup>50</sup>.

The Gradient Boosting and Random Forest Regression based machine learning approach is used to predict the response characteristics i.e., MRR, HOC and CE. The experimental results obtained during UR-ECDD process L16 design at different machining control parameters i.e., ultrasonic vibration, work material rotation, tool feed rate, applied voltage and electrolyte concentration are used for machine learning analysis. The 16 experiments are splitted into a training (9), testing (3) and validation (4) set using the scikit-learn `train_test_split` function that provides the best prediction results. Web search cross-validation is used to find the best hyper parameters of in both the Regressor model separately to predict each target variable. The parameter grid contains options for the number of evaluations, the learning rate and the maximum depth of combination trees. The best model for each target variable is then selected based on the grid search results. Finally, these best models can be used to predict the corresponding processing performance indicators.

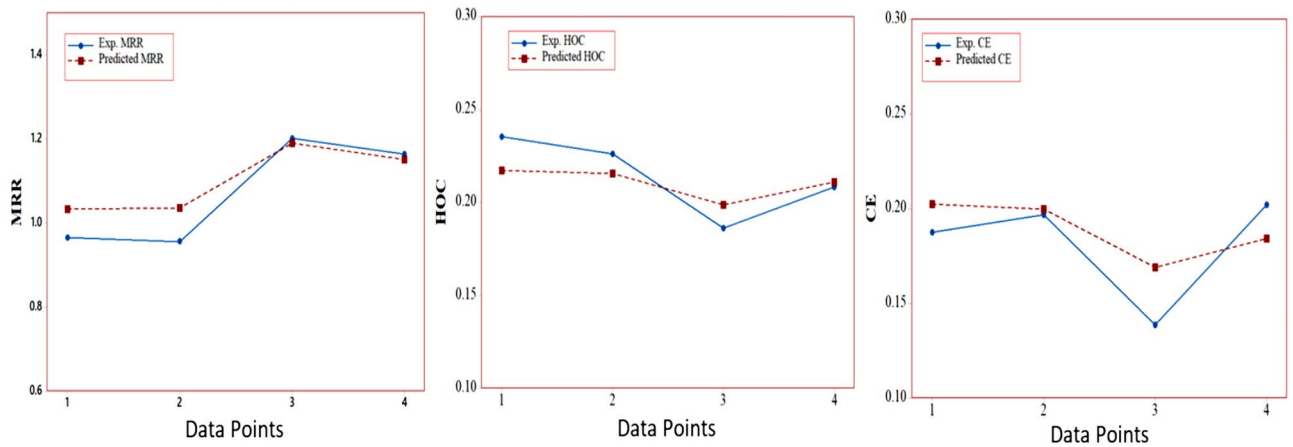
### Results analysis

Figure 16 provides the comparison of experimental and predicted values of the MRR, HOC and CE during training of the model. It is clear from the figure that the predicted values are in close relation with the experimental values predicted through Random Forest regression when compared to Gradient Boost regression model. The predicted model is validated to check the efficacy and used to predict the optimal values of the responses. Figure 17 shows the plot of experimental and predicted values during the validation study in Random Forest Regression. It is observed that the trend of the predicted values is similar to the experimental. However, an error is also observed that may be due to lack of data and overfitting<sup>51</sup>. The ML based study indicates that Random Forest Regression based machine learning approach is better and capable of predicting the responses i.e., MRR, HOC and CE with accuracy.

Both academic and industrial applications can benefit from the findings of ML-based predictive modelling. Researchers can better understand the intricate relationships between the different variables by using this data-driven method to analyse and optimize UR-ECDD machining parameters especially tool vibrations and work material rotations. Additionally, by providing an effective outcome prediction, it lessens the need for lengthy experimental trials. Manufacturers can improve efficiency, accuracy, and overall machining quality in UR-ECDD operations by optimizing process parameters through machine learning in industrial applications. Adaptive control based on projected outcomes is made possible by its support for real-time monitoring and decision-making. By increasing the predictability and repeatability of machining results, it also contributes to sustainability and lessens material waste.



**Fig. 16.** Comparison of predicted and experimental results using random forest and gradient boost (training data set).



**Fig. 17.** Comparison of predicted and experimental results using random forest (validation data set).

## Conclusions

The fundamental purpose of this investigation is to perform a detailed analysis into the multi-criteria optimization of UR-ECDD input factors. With a focus on soda lime glass material, the major objectives of this optimization are to maximise MRR, minimise HAZ and CE during the micro-hole drilling process. The ultimate goal of this investigation is to boost the accuracy and productivity of micro-hole drilling operations by conducting a comprehensive performance evaluation. Two important techniques are used: the signal-to-noise (S/N) ratio and the grey relational analysis (GRA) to systematically analyse the machining performance and determine the optimum range of control variables. Taking into account the MRR, HOC and CE as essential performance measures, these techniques offer a strong framework for evaluating the effectiveness of the UR-ECDD. The investigation's key finding is that the previously difficult multi-criteria optimization issue was simplified into a more doable single-objective optimization work. This simplification is essential to making it easier to evaluate the machining process in a straightforward and efficient manner. By doing this, it emphasises the benefits of using the Grey Relational Analysis (GRA) approach rather than the S/N ratio to get the intended optimization results. The machine learning based predictive model is developed using Gradient Boost and Random Forest approach. The major conclusions withdrawn from the present investigation are:

1. The S/N ratio shows that the best control variable combination for maximizing the MRR is A4C3B1D2E4, corresponding to (3  $\mu\text{m}$ , 80 rpm, 0.6 mm/min, 40 V, 25 wt%), whereas the best combination to minimize the HOC is A4B4C3D3E3, corresponding to (6  $\mu\text{m}$ , 0.9 mm/min, 45 V, 20 wt%) and to minimize CE is A4C2D-1B1E3 corresponding to (6  $\mu\text{m}$ , 80 rpm, 35 V, 0.6 mm/min, 20 wt%) respectively.
2. The tool vibrations and work material rotational effect enhance the response indicators during the drilling process owing to better replenishment of the electrolyte in the drilling region followed by uniform and consistent spark frequency. The rotational effect introduced centrifugal effect that helps in the removal of the debris that further prevents the rupture of the gas film and maintain consistent sparks.
3. GRA based optimized control variables obtained for multi-criteria responses in UR-ECDD is A4C3B4D1E4 (6  $\mu\text{m}$ , 80r pm, 0.9 mm/min, 35 V, 25 wt%).
4. When responses are assessed at the optimum combination of the control variables in contrast to initial control variables, a 42.16% improvement in the GRG is seen.
5. The present investigation can effectively help determine the optimum set of control variables to improve the performance of the ultrasonic assisted rotary electrochemical discharge drilling process. It has proven to be suitable for doing multi-criteria response optimization.
6. UR-ECDD presents a cost-effective alternative to traditional drilling methods, despite its ability to machine hard and brittle materials with improved geometrical accuracies in terms of HOC, CE and efficiency. Reduction in tool wear results in longer tool life that may be able to offset long-term maintenance costs, but the additional equipment (Transducer, Motor for rotation, Tooling and Fixture etc.) needed might result in higher initial setup costs. The increasing quality with UR-ECDD process reduces the cost of post processing. Process may require extra energy to machine the material that leads to increase in operation cost.
7. The proposed Random Forest based machine learning model outperforms Gradient Boost method in terms of prediction accuracy, and robustness, requiring less training data.
8. Random Forest Method is validated to assess its efficacy and predicted values shows a similarity in trend with the experimental values.

## Future scope of the study

UR-ECDD exhibits better geometrical characteristics in terms of circularity and overcut during soda lime glass drilling. However, there are some areas that still can be explored for further improvement of the process as given below:

1. It is observed that during drilling process, tool comes in contact with the work material when it is moving at a higher tool feed rate. The tool contact with the work material deteriorates the surface quality and results in deteriorated hole shape. The future work can be extended by utilizing the load sensor that detect the tool contact with the work material in UR-ECDD process.
2. The evaluation of the thermal effects and machining induced stresses on the material properties can also be the motivation for future work.
3. Researching and investigating the green electrolytes that can reduce the environmental impact in terms of fumes and vapors. It also enhances the safety of the operator. Moreover, the novel filtration techniques for used electrolytes that can help in waste management can be explored.
4. Considering responses like high aspect ratio, cylindricity and hole taperness etc. can also be a work for future study for multi-criteria optimization.
5. The effect of different tool shapes in optimizing drilling performance and tool life.

### Data availability

All data generated or analysed during this study are included in this manuscript. All the characterizations, analysis, testing-related works, and modelings have solely been the responsibility of Sahil Grover, Viveksheel Rajput, and Sandeep Singh. Additionally, the raw data can be obtained on request from the corresponding authors, Sahil Grover, Viveksheel Rajput, and Sandeep Singh.

Received: 2 December 2024; Accepted: 28 February 2025

Published online: 09 May 2025

### References

1. Kurafuji, H. Electrical discharge drilling of glass. *Ann. CIRP*. **16**, 415–419 (1968).
2. Mekaru, H., Okuyama, C. & Ueno, A. Fabrication of glass-like carbon molds to imprint on glass materials by MEMS processing technologies. *Microsyst. Technol.* **19**, 315–323 (2013).
3. Xu, J., Du, Y., Tian, Y. & Wang, C. Progress in wafer bonding technology towards MEMS, high-power electronics, optoelectronics, and optofluidics. *Int. J. Optomechatron.* **14**(1), 94–118 (2020).
4. Zheng, Z. P., Cheng, W. H., Huang, F. Y. & Yan, B. H. 3D microstructuring of Pyrex glass using the electrochemical discharge machining process. *J. Micromech. Microeng.* **17**, 960–966. <https://doi.org/10.1088/0960-1317/17/5/016> (2007).
5. Lee, E. S., Howard, D., Liang, E., Collins, S. D. & Smith, R. L. Removable tubing interconnects for glass-based micro-fluidic systems made using ECDD. *J. Micromech. Microeng.* **14**, 535–541. <https://doi.org/10.1088/0960-1317/14/4/014> (2004).
6. Basak, I. & Ghosh, A. Mechanism of material removal in electrochemical discharge machining: A theoretical model and experimental verification. *J. Mater. Process. Technol.* **71**(3), 350–359 (1997).
7. Kolhekar, K. R. & Sundaram, M. Study of gas film characterization and its effect in electrochemical discharge machining. *Precis. Eng.* **1**(53), 203–211 (2018).
8. Rajput, V., Goud, M. & Suri, N. M. Review on recent advances, research trends, and gas film in electrochemical discharge-based micromachining. *J. Micro Nano Manuf.* **9**(1), 010801 (2021).
9. Rajput, V., Goud, M. & Suri, N. M. Study on effective process parameters: Toward the better comprehension of ECDD process. *Int. J. Mod. Manuf. Tech.* **11**, 105–118 (2019).
10. Bhattacharyya, B., Doloi, B. N. & Sorkhel, S. K. Experimental investigations into electrochemical discharge machining (ECDD) of non-conductive ceramic materials. *J. Mater. Process. Technol.* **95**(1–3), 145–154 (1999).
11. Rajput, V., Pundir, S. S., Goud, M. & Suri, N. M. Multi-response optimization of ECDD parameters for silica (quartz) using grey relational analysis. *Silicon* **13**, 1619–1640 (2021).
12. Rajput, V., Goud, M. & Suri, N. M. Performance analysis on the effect of different electrolytes during glass micro drilling operation using ECDD. *i-Manag. J. Future Eng. Technol.* **14**(4), 5 (2019).
13. Rajput, V., Goud, M. & Suri, N. M. Performance analysis of ECDD process using surfactant mixed electrolyte. In *Manufacturing Engineering: Select Proceedings of CPIE 2019*, 285–300 (Springer, Singapore, 2020).
14. Hung, J. C., Zhang, Y. W. Ultrasonic-assisted electrochemical discharge grinding and broaching for machining quartz square microholes. *J. Mater. Res. Technol.* **25**, 1782–1799 (2023).
15. Rusli, M. & Furutani, K. Performance of micro-hole drilling by ultrasonic-assisted electro-chemical discharge machining. *Adv. Mater. Res.* **8**(445), 865–870 (2012).
16. Grover, S., Mangal, S. K. & Singh, S. Micro-machining and process optimization of ultrasonic assisted rotary  $\mu$ -electrochemical discharge machining using TOPSIS method. *Mater. Today Proc.* **0**, 1–6 (2023).
17. Jain, N. & Jain, J. K. Implementation of tool and electrolyte-based development in the ultrasonic-assisted ECDD process: A review. *J. Braz. Soc. Mech. Sci. Eng.* **44**(6), 248 (2022).
18. Wüthrich, R., Despont, B., Maillard, P. & Bleuler, H. Improving the material removal rate in spark-assisted chemical engraving (SACE) gravity-feed micro-hole drilling by tool vibration. *J. Micromech. Microeng.* **16**(11), N28 (2006).
19. Song, X. F. et al. Ultrasonic assisted high rotational speed diamond machining of dental glass ceramics. *Int. J. Adv. Manuf. Technol.* **96**, 387–399 (2018).
20. Xu, B., Wang, Y., Zhenliang, L. I., Zhu, K., Fan, Y. & Li, H, inventors; Gold Array Technology (Beijing) LLC, assignee. Photo-curing 3D printer and 3D printing method. United States patent US 10399270, 2019 Sep 3.
21. Fan, Z. W. & Hourng, L. W. Electrochemical micro-drilling of deep holes by rotational cathode tools. *Int. J. Adv. Manuf. Technol.* **52**, 555–563 (2011).
22. Grover, S., Singh, S. & Mangal, S. K. Hybridization of  $\mu$ -electrochemical discharge machining ( $\mu$ -ECDD) process: A review. *Mater. Today Proc.* **1**(80), 499–508 (2023).
23. Rajput, V., Goud, M. & Suri, N. M. Enhancement of electrochemical discharge machining (ECDD) characteristics with tool electrode rotation. In *Advances in Modelling and Optimization of Manufacturing and Industrial Systems: Select Proceedings of CIMS 2021*, 135–148 (Springer, Singapore, 2023).
24. Singh, M., Singh, S. & Kumar, S. Experimental investigation for generation of micro-holes on silicon wafer using electrochemical discharge machining process. *Silicon* **12**, 1683–1689 (2020).
25. Gautam, N. & Jain, V. K. Experimental investigations into ECSD process using various tool kinematics. *Int. J. Mach. Tools Manuf.* **38**(1–2), 15–27 (1998).
26. Singh, M. et al. Multi response optimization of ECDD process for generating micro holes in CFRP composite using TOPSIS methodology. *Polymers* **14**(23), 5291 (2022).
27. Rajput, V., Goud, M. & Suri, N. M. Three-dimensional finite element modeling and response surface based multi-response optimization during silica drilling with closed-loop ECDD. *Silicon* **1**, 1–27 (2021).

28. Tiwari, A. K. & Panda, S. S. Optimization of process parameters in ECDC machining using Taguchi based grey relation analysis. *Measurement* **1**(216), 112971 (2023).
29. Wang, T., Liu, Y., Wang, K. & Lv, Z. Investigation on a sustainable composite method of glass microstructures fabrication—electrochemical discharge milling and grinding (ECDCM-G). *J. Clean. Prod.* **10**(387), 135788 (2023).
30. Bindu Madhavi, J. & Hiremath, S. S. Machining and characterization of channels and textures on quartz glass using  $\mu$ -ECDCM process. *Silicon* **11**(6), 2919–2931 (2019).
31. Bellubbi, S. N. S. & Mallick, B. Multi response optimization of ECDCM process parameters for machining of microchannel in silica glass using Taguchi–GRA technique. *Silicon* **14**(8), 4249–4263 (2022).
32. Ab Ghani, S., Muhamad, N. A., Noorden, Z. A., Zainuddin, H. & Ahmad, A. A. Multi-response optimization of the properties of natural ester oil with mixed antioxidants using Taguchi-based methodology. *IEEE Trans. Dielectr. Electr. Insul.* **24**(3), 1674–1684 (2017).
33. Grover, S., *et al.* Experimental investigation for micro-machining of borosilicate glass using ultrasonic assisted rotary electrochemical discharge machining (UA-REDCM) process. *J. Micromech. Microeng.* **34**, 055003 (2024).
34. Rajput, V., Goud, M. & Suri, N. M. Performance analysis of closed-loop electrochemical discharge machining (CLEDCM) during micro-drilling and response surface methodology based multi-response parametric optimisation. *Adv. Mater. Process. Technol.* **8**(2), 1352–1382 (2022).
35. Kumar Gupta, P., Divedi, A. & Kumar, P. Effect of electrolytes on quality characteristics of glass during ECDCM. *Key Eng. Mater.* **29**(658), 141–145 (2015).
36. Kumar, N. & Das, A. K. Machining of micro features through  $\mu$ -ECDCM process and evaluation of surface integrity. *CIRP J. Manuf. Sci. Technol.* **1**(36), 45–56 (2022).
37. <https://www.makeitfrom.com/material-properties/Soda-Lime-Float-Glass>
38. Goud, M. & Sharma, A. K. A three-dimensional finite element simulation approach to analyze material removal in electrochemical discharge machining. *Proc. Inst. Mech. Eng. Part C J. Mech. Eng. Sci.* **231**(13), 2417–2428 (2017).
39. Abdullah, A. B., Sapuan, S. M. & Samad, Z. Roundness error evaluation of cold embossed hole based on profile measurement technique. *Int. J. Adv. Manuf. Technol.* **80**, 293–300 (2015).
40. Tang, L. & Yang, S. J. Experimental investigation on the electrochemical machining of  $00\text{Cr}_{12}\text{Ni}_9\text{Mo}_4\text{Cu}_2$  material and multi-objective parameters optimization. *Int. J. Adv. Manuf. Technol.* **67**, 2909–2916 (2013).
41. Oza, A. D., Kumar, A., Badheka, V. & Arora, A. Traveling wire electrochemical discharge machining (TW-ECDCM) of quartz using zinc coated brass wire: Investigations on material removal rate and kerf width characteristics. *Silicon* **11**, 2873–2884 (2019).
42. Sindhu, D., Thakur, L. & Chandna, P. Multi-objective optimization of rotary ultrasonic machining parameters for quartz glass using Taguchi–Grey relational analysis (GRA). *Silicon* **15**(11), 2033–2044 (2019).
43. Wang, J., Li, P., Ran, R., Che, Y. & Zhou, Y. A short-term photovoltaic power prediction model based on the gradient boost decision tree. *Appl. Sci.* **8**(5), 689 (2018).
44. Chen, Y. *et al.* Performance prediction and parameter optimization of alumina-titanium carbide ceramic micro-EDM hole machining process based on XGBoost. *Proc. Inst. Mech. Eng. Part L J. Mater. Des. Appl.* **238**(2), 310–319 (2024).
45. Abbas, A. T. *et al.* A machine learning perspective to the investigation of surface integrity of Al/SiC/Gr composite on EDM. *J. Manuf. Mater. Process.* **7**(5), 163 (2023).
46. Schapire, R. E. The strength of weak learnability. *Mach. Learn.* **5**, 197–227 (1990).
47. Jafarzadeh, H., Mahdianpari, M., Gill, E., Mohammadimanesh, F. & Homayouni, S. Bagging and boosting ensemble classifiers for classification of multispectral, hyperspectral and PolSAR data: A comparative evaluation. *Remote Sens.* **13**(21), 4405 (2021).
48. Ganjisaffar, Y., Caruana, R. & Lopes, C. V. Bagging gradient-boosted trees for high precision, low variance ranking models. In *Proceedings of the 34th International ACM SIGIR Conference on Research and Development in Information*, 85–94 (Retrieval 2011 Jul 24).
49. Abubakar, Y. & Ahmad, N. B. Prediction of Students’ performance in E-learning environment using random forest. *Int. J. Innov. Comput.* **7**(2), 1–5 (2017).
50. Zhu, M., Yang, Y., Feng, X., Du, Z. & Yang, J. Robust modeling method for thermal error of CNC machine tools based on random forest algorithm. *J. Intell. Manuf.* **34**(4), 2013–2026 (2023).
51. Grzenda, M. & Bustillo, A. The evolutionary development of roughness prediction models. *Appl. Soft Comput.* **13**(5), 2913–2922 (2013).

## Acknowledgements

The authors extend their appreciation to the Deanship of Scientific Research at King Khalid University for funding this work through large group Research Project under grant number RGP2/28/44.

## Author contributions

Conceptualization, SG, VR, SKM, Sarbjit Singh (SS), Sandeep Singh (SS); methodology, SG, VR, SKM, Sarbjit Singh (SS), Sandeep Singh (SS); formal analysis, SG, VR, SKM, Sarbjit Singh (SS), Sandeep Singh (SS), Shubham Sharma (SS); investigation, SG, VR, SKM, Sarbjit Singh (SS), Sandeep Singh (SS); writing—original draft preparation, SG, VR, SKM, Sarbjit Singh (SS), Sandeep Singh (SS); writing—review and editing, Shubham Sharma (SS), EESM, DK, JL; supervision, EESM, DK, JL; project administration, EESM, DK, JL; funding acquisition, EESM, DK, JL. All authors have read and agreed to the published version of the manuscript.

## Funding

The authors extend their appreciation to the Deanship of Scientific Research at King Khalid University for funding this work through large group Research Project under grant number RGP2/28/44.

## Competing interests

The authors declare no competing interests.

## Additional information

**Correspondence** and requests for materials should be addressed to S.S., S.S. or J.L.

**Reprints and permissions information** is available at [www.nature.com/reprints](http://www.nature.com/reprints).

**Publisher’s note** Springer Nature remains neutral with regard to jurisdictional claims in published maps and institutional affiliations.

**Open Access** This article is licensed under a Creative Commons Attribution-NonCommercial-NoDerivatives 4.0 International License, which permits any non-commercial use, sharing, distribution and reproduction in any medium or format, as long as you give appropriate credit to the original author(s) and the source, provide a link to the Creative Commons licence, and indicate if you modified the licensed material. You do not have permission under this licence to share adapted material derived from this article or parts of it. The images or other third party material in this article are included in the article's Creative Commons licence, unless indicated otherwise in a credit line to the material. If material is not included in the article's Creative Commons licence and your intended use is not permitted by statutory regulation or exceeds the permitted use, you will need to obtain permission directly from the copyright holder. To view a copy of this licence, visit <http://creativecommons.org/licenses/by-nc-nd/4.0/>.

© The Author(s) 2025

## Terms and Conditions

Springer Nature journal content, brought to you courtesy of Springer Nature Customer Service Center GmbH (“Springer Nature”).

Springer Nature supports a reasonable amount of sharing of research papers by authors, subscribers and authorised users (“Users”), for small-scale personal, non-commercial use provided that all copyright, trade and service marks and other proprietary notices are maintained. By accessing, sharing, receiving or otherwise using the Springer Nature journal content you agree to these terms of use (“Terms”). For these purposes, Springer Nature considers academic use (by researchers and students) to be non-commercial.

These Terms are supplementary and will apply in addition to any applicable website terms and conditions, a relevant site licence or a personal subscription. These Terms will prevail over any conflict or ambiguity with regards to the relevant terms, a site licence or a personal subscription (to the extent of the conflict or ambiguity only). For Creative Commons-licensed articles, the terms of the Creative Commons license used will apply.

We collect and use personal data to provide access to the Springer Nature journal content. We may also use these personal data internally within ResearchGate and Springer Nature and as agreed share it, in an anonymised way, for purposes of tracking, analysis and reporting. We will not otherwise disclose your personal data outside the ResearchGate or the Springer Nature group of companies unless we have your permission as detailed in the Privacy Policy.

While Users may use the Springer Nature journal content for small scale, personal non-commercial use, it is important to note that Users may not:

1. use such content for the purpose of providing other users with access on a regular or large scale basis or as a means to circumvent access control;
2. use such content where to do so would be considered a criminal or statutory offence in any jurisdiction, or gives rise to civil liability, or is otherwise unlawful;
3. falsely or misleadingly imply or suggest endorsement, approval, sponsorship, or association unless explicitly agreed to by Springer Nature in writing;
4. use bots or other automated methods to access the content or redirect messages
5. override any security feature or exclusionary protocol; or
6. share the content in order to create substitute for Springer Nature products or services or a systematic database of Springer Nature journal content.

In line with the restriction against commercial use, Springer Nature does not permit the creation of a product or service that creates revenue, royalties, rent or income from our content or its inclusion as part of a paid for service or for other commercial gain. Springer Nature journal content cannot be used for inter-library loans and librarians may not upload Springer Nature journal content on a large scale into their, or any other, institutional repository.

These terms of use are reviewed regularly and may be amended at any time. Springer Nature is not obligated to publish any information or content on this website and may remove it or features or functionality at our sole discretion, at any time with or without notice. Springer Nature may revoke this licence to you at any time and remove access to any copies of the Springer Nature journal content which have been saved.

To the fullest extent permitted by law, Springer Nature makes no warranties, representations or guarantees to Users, either express or implied with respect to the Springer nature journal content and all parties disclaim and waive any implied warranties or warranties imposed by law, including merchantability or fitness for any particular purpose.

Please note that these rights do not automatically extend to content, data or other material published by Springer Nature that may be licensed from third parties.

If you would like to use or distribute our Springer Nature journal content to a wider audience or on a regular basis or in any other manner not expressly permitted by these Terms, please contact Springer Nature at

[onlineservice@springernature.com](mailto:onlineservice@springernature.com)